



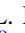









Revisiting the Transit Timing Variations in the TrES-3 and Qatar-1 Systems with TESS Data

Vineet Kumar Mannaday^{1,2} , Parijat Thakur¹ , John Southworth³ , Ing-Guey Jiang⁴ , D. K. Sahu⁵ , L. Mancini^{6,13,14,15} ,
M. Vaňko⁷ , Emil Kundra⁷ , Pavol Gajdoš⁸ , Napaporn A-thano⁴, Devesh P. Sariya⁴ , Li-Chin Yeh⁹, Evgeny Griv¹⁰,
David Mkrtychian¹¹, and Aleksey Shlyapnikov¹²

¹ Department of Pure and Applied Physics, Guru Ghasidas Vishwavidyalaya (A Central University), Bilaspur (C.G.) 495009, India; parijat@associates.iucaa.in, parijatthakur@yahoo.com

² Department of Physics, Govt. Niranjan Kesharwani College, Kota, Bilaspur (C.G.) 495113, India

³ Astrophysics Group, Keele University, Staffordshire, ST5 5BG, UK

⁴ Department of Physics and Institute of Astronomy, National Tsing-Hua University, Hsinchu 30013, Taiwan

⁵ Indian Institute of Astrophysics, Bangalore 560 034, India

⁶ Department of Physics, University of Rome Tor Vergata, Viadella Ricerca Scientifica 1, I-00133, Rome, Italy

⁷ Astronomical Institute, Slovak Academy of Sciences, SK-059 60 Tatranská Lomnica, Slovakia

⁸ Institute of Physics, Faculty of Science, Pavol Jozef Šafárik University, 040 01 Košice, Slovakia

⁹ Institute of Computational and Modeling Science, National Tsing-Hua University, Hsinchu 30013, Taiwan

¹⁰ Department of Physics, Ben-Gurion University, Beer-Sheva 84105, Israel

¹¹ National Astronomical Research Institute of Thailand (NARIT), Siripanich Building, 191 Huaykaew Road, Muang District, Chiangmai, 50180, Thailand

¹² Crimean Astrophysical Observatory, 298409, Nauchny, Crimea[†]

¹³ Max Planck Institute for Astronomy, Königstuhl 17, D-69117 Heidelberg, Germany

¹⁴ INAF – Osservatorio Astrofisico di Torino, via Osservatorio20, I-10025, Pino Torinese, Italy

¹⁵ International Institute for Advanced Scientific Studies (IIASS), Via G. Pellegrino 19, I-84019, Vietri sul Mare (SA), Italy

Received 2022 July 5; revised 2022 August 20; accepted 2022 September 8; published 2022 October 18

Abstract

We present and analyze 58 transit light curves of TrES-3b and 98 transit light curves of Qatar-1b, observed by the Transiting Exoplanet Survey Satellite, plus two transit light curves of Qatar-1b, observed by us, using a ground-based 1.23 m telescope. These light curves are combined with the best-quality light curves taken from the Exoplanet Transit Database and the literature. The precisely determined midtransit times from these light curves enable us to obtain the refined orbital ephemerides, with improved precision, for both hot Jupiters. From the timing analysis, we find indications of the presence of transit timing variations (TTVs) in both systems. Since the observed TTVs are unlikely to be short-term and periodic, the possibility of additional planets in orbits close to TrES-3b and Qatar-1b is ruled out. The possible causes of long-term TTVs, such as orbital decay, apsidal precession, the Applegate mechanism, and line-of-sight acceleration, are also examined. However, none of these possibilities are found to explain the observed TTV of TrES-3b. In contrast to this, line-of-sight acceleration appears to be a plausible explanation for the observed TTV of Qatar-1b. In order to confirm these findings, further high-precision transit and radial velocity observations of both systems would be worthwhile.

Unified Astronomy Thesaurus concepts: Exoplanets (498); Hot Jupiters (753); Tidal interaction (1699); Transit photometry (1709); Transit timing variation method (1710); Radial velocity (1332)

Supporting material: machine-readable tables

1. Introduction

The photometric study of transiting hot-Jupiter systems is important for several reasons, because it not only helps in improving estimates of their physical and orbital parameters, but also provides an opportunity to check for the presence of an additional body in the system through the transit timing variation (TTV) analysis of a known planet (see Jiang et al. 2013; Maciejewski et al. 2013; Collins et al. 2017; Mannaday et al. 2020; Sariya et al. 2021; Su et al. 2021; A-thano et al. 2022). Moreover, long-term high-precision transit data spanning more than a decade allows tests of the theoretical predictions of orbital decay and

apsidal precession in hot-Jupiter systems (e.g., Maciejewski et al. 2016; Patra et al. 2017; Mannaday et al. 2020; Patra et al. 2020; A-thano et al. 2022). Orbital decay is predicted for most hot Jupiters, because the total angular momentum of such a system is smaller than the critical angular momentum that is required for a system to achieve a stable state (see Rasio et al. 1996; Levrard et al. 2009; Matsumura et al. 2010). As the orbital frequency of most hot Jupiters is larger than the host star's rotational frequency, the tidal bulges raised on the host stars by their hot Jupiters exert torque that leads to orbital decay, by transferring the planet's orbital angular momentum to the stellar rotational angular momentum (Jackson et al. 2009; Levrard et al. 2009; Matsumura et al. 2010). On the other hand, apsidal precession is expected in systems whose hot Jupiters are in at least slightly eccentric ($e > 0.003$) orbits (Ragozzine & Wolf 2009). The tidal bulge raised on the planet by the host star also exerts torque on the orbit, which can lead to apsidal precession (see Ragozzine & Wolf 2009). Probing these two phenomena provides an opportunity to infer significant information about the hot-Jupiter systems. The orbital decay rate allows the estimation of the modified stellar tidal quality factor

[†] While the AAS journals adhere to and respect UN resolutions regarding the designations of territories (available at <http://www.un.org/press/en>), it is our policy to use the affiliations provided by our authors on published articles.

(Q_*), a dimensionless parameter that describes the efficiency of the energy dissipation in the host star, which is still poorly constrained by observations. The observed apsidal precession rate provides an opportunity to infer the interior density profile of a planet by estimating the planetary tidal Love number (k_p ; see Ragozzine & Wolf 2009; Patra et al. 2017; Bouma et al. 2019; Mannaday et al. 2020).

In order to address these issues, the Transiting Exoplanet Survey Satellite (TESS; Ricker et al. 2014), which launched in 2018, is valuable, because it is not only discovering new extrasolar planets, but also following up the transits of previously known hot Jupiters. Combining ground-based transit data with the high-precision 2 minute cadence transit data provided by TESS is extremely helpful for refining the estimates of system parameters (e.g., Cortés-Zuleta et al. 2020; Ikwut-Ukwa et al. 2020; Szabó et al. 2020; Southworth et al. 2022), exploring the existence of additional planets (e.g., Huang et al. 2018; Garai et al. 2020; Teske et al. 2020), and searching for the possibility of long-term trends due to orbital decay, apsidal precession, the Applegate mechanism (Applegate 1992), and line-of-sight acceleration phenomena in hot-Jupiter systems (e.g., Watson & Marsh 2010; Bouma et al. 2019; Southworth et al. 2019; Bouma et al. 2020; Yee et al. 2020; Battley et al. 2021; Turner et al. 2021, 2022; Wong et al. 2022). In the context of orbital decay studies, Maciejewski et al. (2016) first reported an orbital decay rate of $-25.60 \pm 4.0 \text{ ms yr}^{-1}$ for the hot Jupiter WASP-12b, using transit data spanning a decade. Patra et al. (2017) confirmed this, but suspected the possibility of apsidal precession. Recent timing analyses performed by Yee et al. (2020), Turner et al. (2021), and Wong et al. (2022), including data from TESS and from the literature, provide strong evidence of orbital decay for WASP-12b. The WASP-12 system is currently the only system in which orbital decay has been confirmed directly through transit observations. The second hot Jupiter for which orbital decay has been detected with high significance, but has not yet been confirmed, is WASP-4b. Using the observed TESS transits and previously published data, Bouma et al. (2019) reported an orbital decay rate of $-12.6 \pm 1.2 \text{ ms yr}^{-1}$ and ~ 80 s early arrivals of the transits of WASP-4b. Southworth et al. (2019) found a similar decay rate for this hot Jupiter using TESS and extensive new ground-based data. Apart from this, they also examined various possible origins of the TTVs, such as stellar activity, the Applegate mechanism, apsidal precession, and line-of-sight acceleration. While orbital decay and apsidal precession were plausible, the other possibilities were ruled out. Later, a timing and radial velocity (RV) analysis performed by Bouma et al. (2020) suggested that the observed decay rate was actually caused by the acceleration of WASP-4b toward the Earth. However, Turner et al. (2022) reanalyzed all the TESS, RV, and literature data, and did not see any indications of the acceleration of WASP-4b toward the Earth, but instead found evidence for the presence of a second planet in the system. In addition to WASP-12b and WASP-4b, there are many hot Jupiters for which a tentative detection of orbital decay has been reported (e.g., WASP-43b: Jiang et al. 2016; WASP-46b: Petrucci et al. 2018), but has yet to be confirmed, either due to contradictory findings (e.g., WASP-43b: Hoyer et al. 2016b; Patra et al. 2020; WASP-46: Davoudi et al. 2021) or due to a lack of observations over sufficient time spans (e.g., KELT-16b, HATS-18b, WASP-18b, WASP-19b, WASP-72b: Patra et al. 2020; Mancini et al. 2022).

In this paper, we have chosen two hot Jupiters, TrES-3b and Qatar-1b, for our timing analysis. The availability of long-term

transit data and additional follow-up observations obtained by previous workers are the main reasons for selecting these two systems. TrES-3b was discovered by the Trans-Atlantic Exoplanet Survey (O’Donovan et al. 2007), orbiting a G-type star ($V = 12.4 \text{ mag}$, $T_{\text{eff}} = 5720 \pm 150$, $M_* = 0.9 \pm 0.15 M_{\odot}$, $R_* = 0.802 \pm 0.046 R_{\odot}$). Qatar-1b was discovered by the Qatar Exoplanet Survey (Alsubai et al. 2011), around a metal-rich K-type star ($V = 13.5 \text{ mag}$, $T_{\text{eff}} = 4861 \pm 125 \text{ K}$, $M_* = 0.85 M_{\odot}$, $R_* = 0.823 \pm 0.025 R_{\odot}$). The transits of both hot Jupiters have been extensively studied in the past, to characterize their physical and orbital properties, as well as to examine the presence of additional planets through TTV analysis (e.g., TrES-3b: Gibson et al. 2009; Sozzetti et al. 2009; Jiang et al. 2013; Kundurthy et al. 2013; Vaňko et al. 2013; Püsküllü et al. 2017; Ricci et al. 2017; Qatar-1b: Covino et al. 2013; von Essen et al. 2013; Maciejewski et al. 2015; Mislis et al. 2015; Collins et al. 2017; Thakur et al. 2018). Recently, Mannaday et al. (2020) examined the TrES-3 system using 12 new transit light curves, with 71 transit light curves from the literature, and discussed the possibilities of orbital decay and apsidal precession phenomena for the observed TTV. Because of a statistically insignificant estimation of the orbital decay rate ($\dot{P}_q = -4.1 \pm 3.1 \text{ ms yr}^{-1}$), they proposed that new data observed by TESS may be useful for confirming their findings. The presence of TTVs has also been reported in the Qatar-1 system by Su et al. (2021), using 38 transit light curves. These authors also found a statistically insignificant period decrease of $(-5.9 \pm 5.2) \times 10^{-10} \text{ day epoch}^{-1}$. Because of this, they proposed further follow-up observations of the transits of Qatar-1b to refine their results.

In the context of the discussion above, we note that TESS has observed TrES-3 and Qatar-1 in multiple sectors (sectors 25, 26, and 40 for TrES-3, and sectors 17, 21, 24, 25, 41, and 48 for Qatar-1). We have processed and analyzed these new transit data to further probe the possible TTVs for both hot Jupiters. As well as the TESS light curves, we have collected further transit light curves from the Exoplanet Transit Database (ETD; Poddany et al. 2010)¹⁶ and the literature, to increase the baseline of the transit observations. Two more transit light curves of Qatar-1b were observed by us using a 1.23 m telescope. In total, 182 transit light curves of TrES-3b and 228 transit light curves of Qatar-1b, spanning more than decade, are employed in this work.

The remainder of this paper is organized as follows. Section 2 presents the ground-based and TESS observations, as well as transit data taken from the ETD and the literature. Section 3 describes the procedure adopted for analyzing the transit data, and the timing analyses are given in Section 4. The results of this analysis are discussed in Section 5, and concluding remarks are given in Section 6.

2. Observational Data

2.1. Ground-based Observations

Two transits of Qatar-1b were observed by us on 2016 August 17 and 2017 March 18 using the 1.23 m Zeiss telescope at the Calar Alto Observatory (CAHA) in Spain. We used the DLR MKIII 4k \times 4k CCD camera, which has pixels of size $15 \mu\text{m}$ and gives a field of view of $21.5 \times 21.5 \text{ arcmin}^2$. The observations were performed with the telescope being defocused, to increase

¹⁶ <http://var2.astro.cz/ETD/>

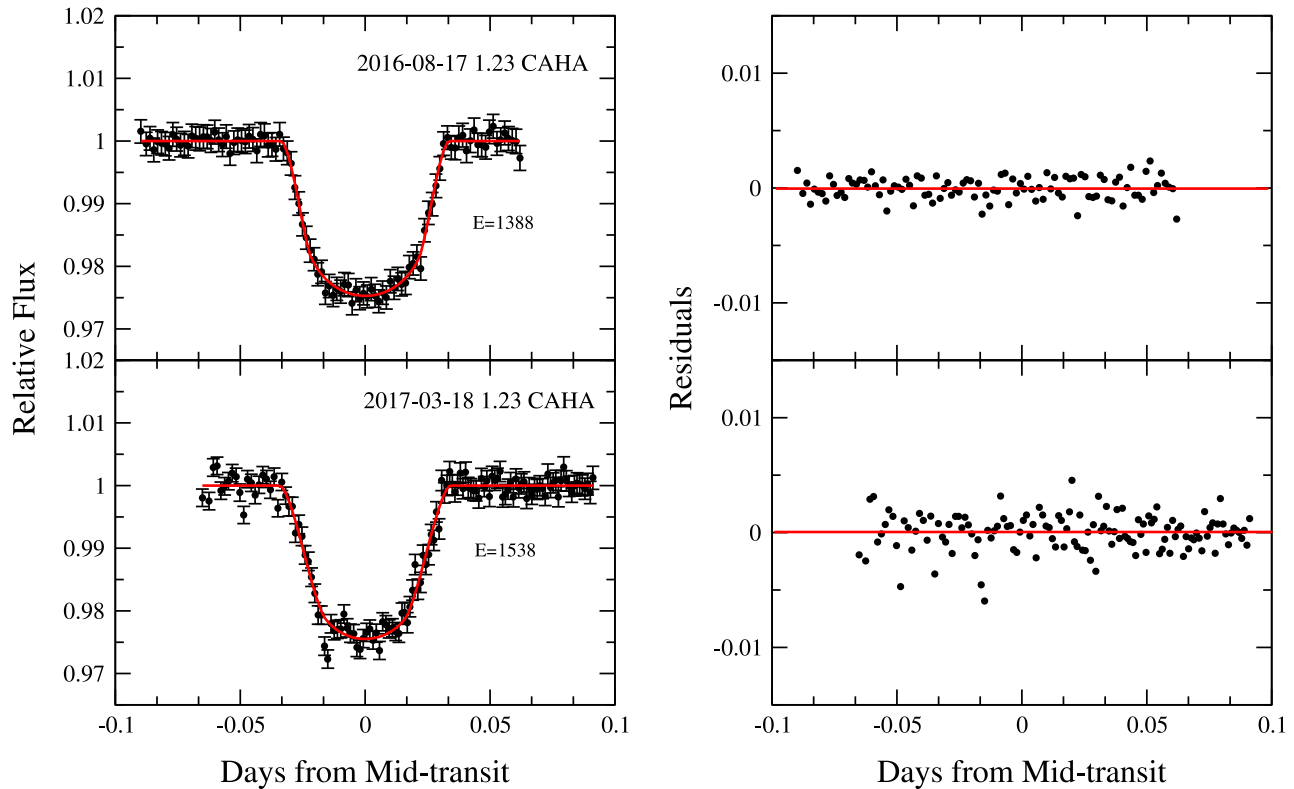


Figure 1. Left panel: the normalized relative flux of Qatar-1 as a function of the time (the offset from the midtransit time and in TDB-based BJD) of two transits observed by us with the 1.23 m telescope at CAHA. The points show the data and the solid lines show the best-fit models. Right panel: the corresponding residuals.

the photometric precision (Southworth et al. 2009a), and with autoguiding. The CCD camera was windowed, to decrease the dead time between exposures. Both transits were observed through a Cousins R filter, which was chosen as it is part of a well-known photometric system and had a high throughput for Qatar-1. The data were reduced in the standard way, using the IDL DEFOT pipeline (Southworth et al. 2009a, 2014). We obtained bias and flat-field calibrations, but did not use them, as they had little effect on the final light curve, apart from adding a small amount of extra noise (see Southworth et al. 2014, 2019). We performed aperture photometry, with apertures being placed manually on a reference image and tracked to follow the stars, by cross-correlating each image with the reference image. The resulting light curves were normalized to zero magnitude by simultaneously fitting a straight line to the out-of-transit (OOT) data and optimizing the weights of a set of comparison stars to minimize the scatter in the data taken outside transit. The time stamps were converted from Heliocentric Julian Day (HJD) to Barycentric Julian Day (BJD) on the Barycentric Dynamical Time (TDB) timescale, using IDL procedures from Eastman et al. (2010).¹⁷ The normalized light curves are shown in Figure 1 (see Section 3 for details), and the original data points are listed in Table 1.

2.2. TESS Observations

TESS observed 58 transits of TrES-3b and 98 transits of Qatar-1b up to sector 48. TrES-3 and Qatar-1 are designated as TIC 116264089 and TIC 236887394, respectively, in the TESS input catalog (see Stassun et al. 2019; Paegert et al. 2021).¹⁸

The science images taken by TESS were reduced to light curves by the Science Processing Operation Center at NASA Ames (Jenkins et al. 2016). For this work, the Presearch Data Conditioning (PDC) light curves, optimized to remove instrumental variability through the method discussed by Smith et al. (2012) and Stumpe et al. (2012, 2014), were directly retrieved from the Mikulski Archive for Space Telescopes,¹⁹ using the JULIET package (Espinoza et al. 2019). Since JULIET has a function to discard the data points of nonzero quality flags, while extracting the time series data (times, fluxes, and flux errors) from the PDC light curve, only the data associated with zero quality flags were retrieved for our analysis (e.g., Huber et al. 2022). The format of the time of the observations, which was initially in TESS Julian Day (TJD_{TDB}), was converted to BJD_{TDB} by adding 2,457,000 (Tenenbaum & Jenkins 2018).

To remove the trends that appear in the time series data of TrES-3 and Qatar-1, the OOT fluxes were modeled through a Gaussian Process (GP), by masking the in-transit points using the transit ephemeris of TrES-3b and Qatar-1b from Mannaday et al. (2020) and Maciejewski et al. (2015), respectively. For this modeling, we used the JULIET package and employed a CELERITE (approximate) Matérn multiplied by exponential kernel (Espinoza et al. 2019). The parameters of the mean out of flux (mflux), the jitter (in parts per million) added in quadrature to the errorbars of the instrument (σ_{ω}), the amplitude of the GP (σ_{mGP}), and the timescale of the Matérn part of the GP (ρ_{mGP}) were fitted freely, while the dilution factor for the photometric noise (mdilution) was fixed to unity. The prior distributions for the parameters σ_{ω} , σ_{mGP} , and ρ_{mGP}

¹⁷ astroutils.astronomy.ohio-state.edu/time/hjd2bjd.html

¹⁸ <https://exo.mast.stsci.edu>

¹⁹ <https://archive.stsci.edu/>

Table 1
The Transit Light-curve Data of TrES-3b and Qatar-1b Considered in This Work

Object Name	Telescope	Epoch	TDB-based BJD	Normalized Flux	Normalized Flux Error
TrES-3	TESS	3674	2458984.70755	0.99676	0.00380
TrES-3	TESS	3674	2458984.70894	0.99744	0.00380
TrES-3	TESS	3674	2458984.71033	1.00183	0.00380
TrES-3	TESS	3675	2458986.01314	1.00439	0.00378
TrES-3	TESS	3675	2458986.01591	0.99716	0.00378
TrES-3	TESS	3675	2458986.01730	0.99884	0.00377
Qatar-1	CAHA	1388	2457618.53719	1.00153	0.00186
Qatar-1	CAHA	1388	2457618.53932	0.99953	0.00186
Qatar-1	CAHA	1388	2457618.54084	1.00043	0.00188
Qatar-1	CAHA	1538	2457831.56558	0.99806	0.00139
Qatar-1	CAHA	1538	2457831.56825	0.99752	0.00139
Qatar-1	CAHA	1538	2457831.56994	1.00289	0.00140
Qatar-1	TESS	2196	2458765.90522	0.99846	0.00384
Qatar-1	TESS	2196	2458765.90660	0.99770	0.00386
Qatar-1	TESS	2196	2458765.90799	0.99665	0.00385
Qatar-1	TESS	2197	2458767.32326	0.99849	0.00385
Qatar-1	TESS	2197	2458767.32465	1.00145	0.00385
Qatar-1	TESS	2197	2458767.32604	0.99830	0.00386

(This table is available in its entirety in machine-readable form.)

were assumed to be uniform, whereas a normal distribution was assumed for mflux (see Espinoza et al. 2019).²⁰ The detrended normalized light curves were obtained by dividing the best-fitting GP model flux by the time series data of each sector. As a reference, the trend of the time series data (top panels), the best-fitting GP model flux to the OOT data (middle panels), and the detrended times series data (bottom panels) of TrES-3 (for sector 25) and Qatar-1 (for sector 17) are shown in Figures 2 and 3, respectively. In order to obtain individual TESS light curves for each transit event of a particular sector, we extracted sections of the detrended normalized light curve within ± 0.1 day around the expected midtransit times. The extracted light curves of TrES-3 and Qatar-1 are depicted by the black points in Figures A1–A5 (see the Appendix). The original data points of these figures are given in Table 1.

2.3. Observational Data from ETD and the Literature

In addition to the TESS and CAHA data, 41 transit light curves of TrES-3b and 61 transit light curves of Qatar-1b were taken from the ETD. We included those with a quality index < 3 . All the ETD light curves were observed between 2016 and 2021 by several observers at different observatories across the world. As most of the ETD light curves were not normalized, we normalized them by fitting a linear function of time to the OOT parts, and also converted their time stamps from JD or HJD to BJD_{TDB}, using the same tool as discussed above. Apart from these light curves, published light curves of both targets available in the literature or available to us were also considered. The details of all the transit light curves of both hot Jupiters employed in this paper are given in Table 2.

3. Light-curve Analysis

To analyze the transit light curves of TrES-3b and Qatar-1b, we used the Transit Analysis Package (TAP; Gazak et al. 2012). All the light curves of each system were loaded into TAP, separately, to determine the transit parameters, such as the ratio of the planet to the star radius (R_p/R_*), the midtransit time (T_m), the orbital inclination (i), the scaled semimajor axis (a/R_*), and the linear and quadratic limb-darkening (LD) coefficients (u_1, u_2). For each light-curve analysis, we used five Markov Chain Monte Carlo (MCMC) chains, with lengths of 10^5 links each, and adopted exactly the same parameter-fitting procedures as described in Mannaday et al. (2020), for TrES-3b, and in Su et al. (2021), for Qatar-1b. To start the TAP run, the initial values of the parameters R_p/R_* , i , and a/R_* were taken from Sozzetti et al. (2009), for TrES-3, and from Maciejewski et al. (2015), for Qatar-1.

For the TESS light curves of TrES-3b and Qatar-1b, the values of the linear and quadratic LD coefficients (u_1, u_2) were taken from the tables of Claret (2017). In the case of the ETD light curves for TrES-3b observed in the clear, V , I , and R filters, the values of u_1 and u_2 were directly adopted from Table 4 of Mannaday et al. (2020), who derived these coefficients using the JKTLD²¹ code (Southworth 2015). For the light curves of Qatar-1b observed in the V , R , and I filters, we followed Su et al. (2021) and linearly interpolated the values of u_1 and u_2 from the tables of Claret & Bloemen (2011), using the EXOFAST²² package (Eastman et al. 2013) with the stellar parameters of effective temperature ($T_{\text{eff}} = 4910$ K), surface gravity ($\log g = 4.55$), and metallicity ($[\text{Fe}/\text{H}] = 0.2$) (Covino et al. 2013; Maciejewski et al. 2015). Since a clear filter covers the V and R bands, the LD coefficients for the light curves of Qatar-1b observed through a clear filter were taken as the

²⁰ <https://juliet.readthedocs.io/en/latest/tutorials/gps.html>

²¹ JKTLD is available from <http://www.astro.keele.ac.uk/jkt/codes.html>.

²² <https://astrouitools.astronomy.osu.edu/exofast/limbdark.shtml>

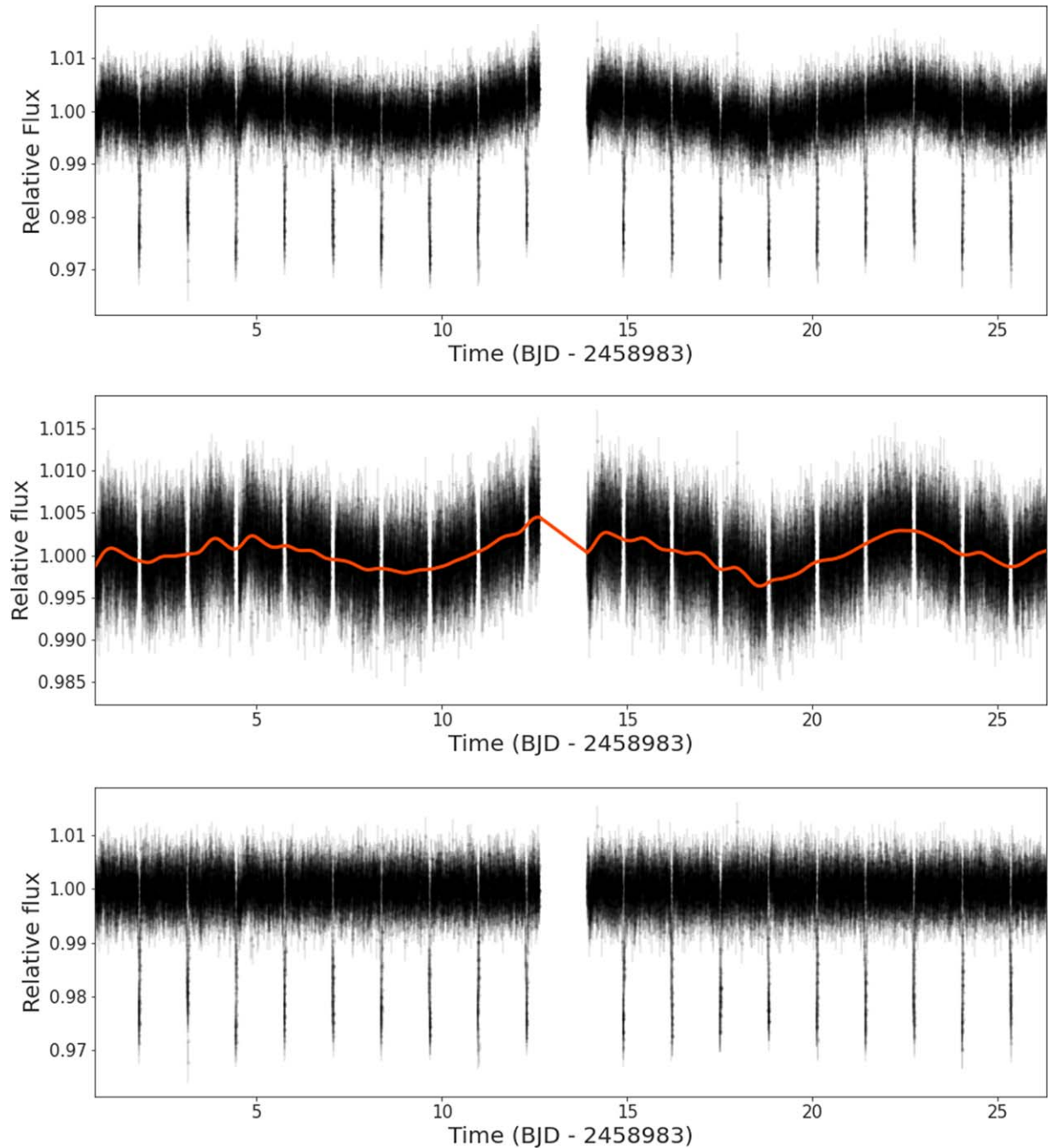


Figure 2. Top panel: time series data of TrES-3b observed by TESS within sector 25. Middle panel: corresponding OOT time series data along with the best-fitting GP model (red curve). Bottom panel: detrended time series data corresponding to the top panel.

average of their values in the V and R filters (see Maciejewski et al. 2013; Mannaday et al. 2020). For the light curves of Qatar-1b observed using the Gunn g , r , and z filters by Mislis et al. (2015), the values of the LD coefficients calculated for the Sloan Digital Sky Survey g , r , and z filters, respectively, were used. We followed Collins et al. (2017) and used the values of the LD coefficients that were calculated with the Kepler and R filters for their Clear with Blue Block (CBB; a high pass filter with cutoff at ~ 500 nm) and an open filter, respectively. To maintain the homogeneity in analyzing and deriving the transit parameters with the transit parameters obtained in Mannaday et al. (2020) and Su et al. (2021), the different packages were used to calculate the LD coefficients for TrES-3 and Qatar-1

stars. The initial values of the LD coefficients used for TrES-3 and Qatar-1 for different filters are listed in Table 3.

After the successful completion of an MCMC run of TAP, the initial 10% of the drawn samples of the model parameters were discarded, as the burn-in stage, and the remaining samples of the model parameters were used for Bayesian parameter extraction. The 50th percentile level (median) of the posterior probability distribution for each model parameter was interpreted as the best-fit value. Moreover, the 15.9 and 84.1 percentile levels (i.e., the 68% credible intervals) of the posterior probability distribution were taken to be the lower and upper 1σ uncertainties, respectively. The values of the model parameters R_p/R_* , T_m , i , a/R_* , u_1 , u_2 , and their 1σ uncertainties derived

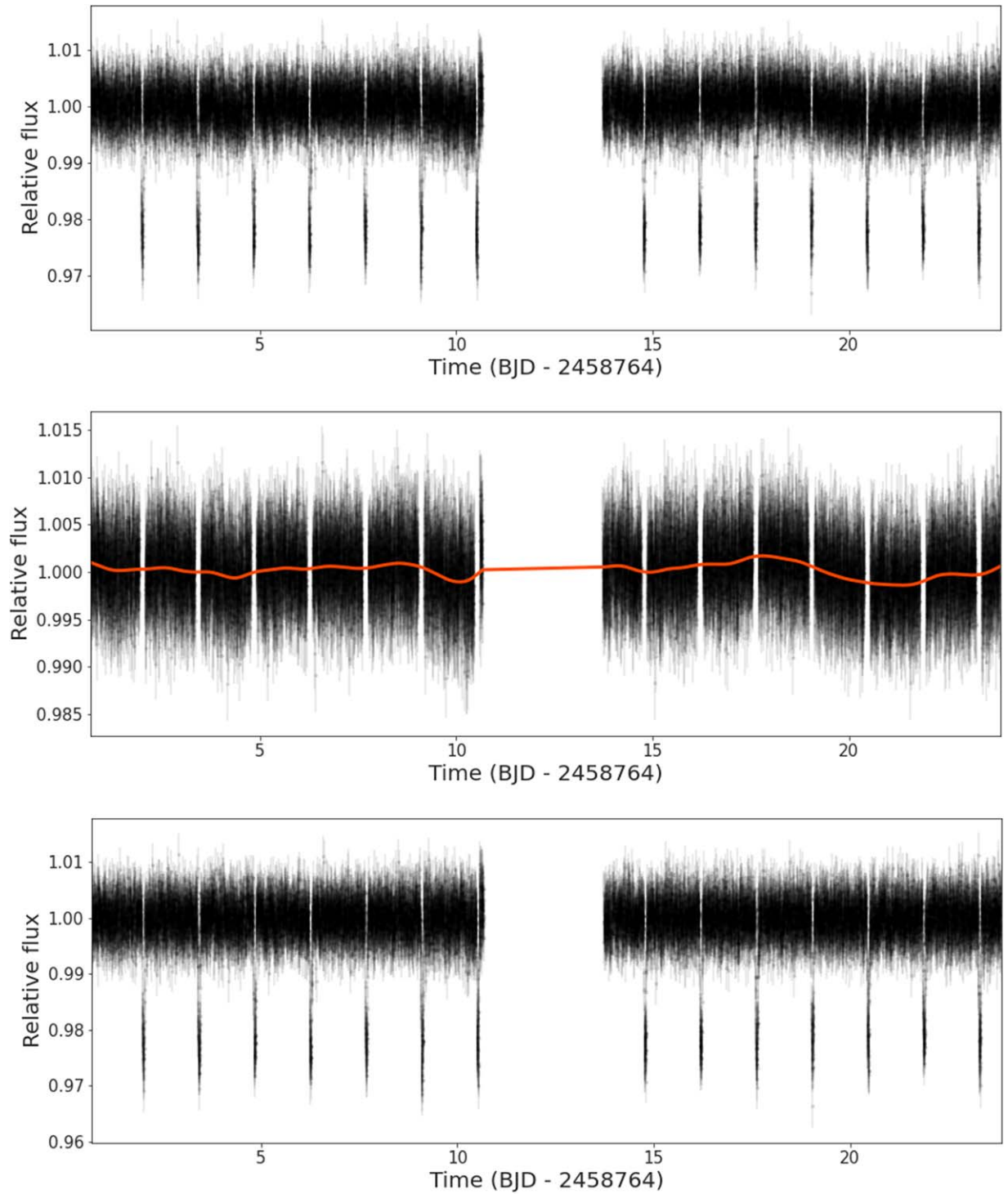


Figure 3. Top panel: time series data of Qatar-1b observed by TESS within sector 17. The remaining panels are the same as those mentioned in Figure 2.

from the TESS light curves of TrES-3b are given in Table 4, whereas those derived from our light curves and the TESS light curves of Qatar-1b are given in Table 5. The red curves overplotted in the left panels of Figure 1 and Figures A1–A5 are the best-fit transit models. To perform a homogeneous and precise timing analysis (e.g., Petrucci et al. 2018; Mannaday et al. 2020), 83 midtransit times of TrES-3b and 38 midtransit times of Qatar-1b were directly taken from Mannaday et al. (2020) and Su et al. (2021), respectively. The midtransit times of TrES-3b and Qatar-1b derived in this paper, along with those

taken from Mannaday et al. (2020) and Su et al. (2021), are gathered in Tables 6 and 7, respectively.

4. Transit Timing Analysis

4.1. New Ephemeris

Although 182 midtransit times of TrES-3b and 228 midtransit times of Qatar-1b are listed in Tables 6–7, we have selected midtransit times with uncertainties less than 1 minute for precise timing analysis (e.g., Maciejewski et al. 2013;

Table 2
Details of the Transit Light Curves of TrES-3b and Qatar-1b Considered in This Work

Object Name	Number of Light Curves Taken	Sources	Total Number of Light Curves
TrES-3b	58	TESS	182
	41	ETD (Poddaný et al. 2010)	
	83	Mannaday et al. (2020)	
Qatar-1b	98	TESS	228
	2	Our observations	
	61	ETD (Poddaný et al. 2010)	
	11	Mislis et al. (2015)	
	18	Collins et al. (2017)	
	38	Su et al. (2021)	

Table 3
The Theoretical LD Coefficients

Object Name	Filter	u_1	u_2
TrES-3	V^a	0.4378	0.2933
	R^a	0.3404	0.3190
	I^a	0.2576	0.3186
	clear ^a	0.3891	0.3062
	TESS ^b	0.3799	0.2051
Qatar-1	V^c	0.6971	0.0880
	R^c	0.5579	0.1600
	I^c	0.4304	0.1962
	Sloan g^c	0.8403	-0.0061
	Sloan r^c	0.5949	0.1479
	Sloan z^c	0.3715	0.2110
	Clear ^d	0.6275	0.1240
	CBB (Kepler filter) ^c	0.6025	0.1291
	TESS ^b	0.4518	0.1870

Notes.

^a u_1 and u_2 are directly adopted from Mannaday et al. (2020).

^b u_1 and u_2 are taken from the tables of Claret (2017).

^c Calculated using EXOFAST, with $T_{\text{eff}} = 4910$ K, $\log g = 4.55$, and $[\text{Fe}/\text{H}] = 0.2$.

^d Calculated as the average of the value in the V and R filters.

Petrucci et al. 2018; Shan et al. 2021). A total of 129 midtransit times of TrES-3b and 184 midtransit times of Qatar-1b passed this selection criterion.

We derived new linear ephemerides for both hot Jupiters by fitting a linear model,

$$T_m^c(E) = T_0 + EP, \quad (1)$$

to their precise midtransit times as a function of epoch E , using the *emcee* MCMC sampler implementation (Foreman-Mackey et al. 2013), where T_m^c , E , P , and T_0 are the calculated midtransit time, epoch, orbital period, and midtransit time of the reference epoch ($E = 0$),²³ respectively. To run the MCMC chain for model fitting, we followed Mannaday et al. (2020) and assumed a Gaussian likelihood, as well as imposing uniform priors on the model parameters, P and T_0 (see Table 8).

²³ The first transits of TrES-3b and Qatar-1b observed by Sozzetti et al. (2009) and von Essen et al. (2013) were considered as $E = 0$, respectively.

We used 100 walkers and ran 300 steps per walker as the initial burn-in to set the step size of each parameter. Following this, the code was further run for a final 20,000 steps per walker, to sample the posterior probability distributions of the model parameters. In order to assess the convergence and sampling of the MCMC chains, we estimated the mean acceptance fraction (a_f), the integrated autocorrelation time (τ), and the effective number of independent samples (N_{eff}), which are listed in Table 8. These parameters indicate efficient convergence and good sampling of the MCMC chains, as the estimated value of a_f lies within the ideal range of 0.2–0.5 and the value of N_{eff} is found to be larger than its minimum threshold value of 50 per walker, as set in our MCMC analysis (see Goodman & Weare 2010; Foreman-Mackey et al. 2013; Cloutier & Triaud 2016; Stefansson et al. 2017; Mannaday et al. 2020).

Before performing the Bayesian parameter extraction from the drawn samples of the posterior probability distributions, we discarded $\sim 2\tau$ steps from the 20,000 steps of each walker, as a final burn-in, to get rid of the strongly correlated parameters. The median and 68% credible intervals of the remaining samples of the posterior probability distribution of each model parameter are considered as the best-fit value and the lower and upper 1σ uncertainties. The best-fit parameters and the 1σ uncertainties derived from the linear model fitting are listed in Table 8 for both targets. Moreover, the obtained values of χ^2 , χ_{red}^2 , and the the Bayesian Information Criterion ($\text{BIC} = \chi^2 + k \log N$, where k is the number of free parameters and N is the number of data points) corresponding to the best-fit model parameters are also listed in this table. The derived values of linear ephemeris for both the hot Jupiters are consistent with the results available in the literature. However, they are estimated with improved precision. Comparing the midtransit times of TrES-3b derived from the TESS light curves with those estimated using the linear ephemeris of Mannaday et al. (2020), we have found a median difference of ~ 32.26 s between these two timings. From this, it appears that the TESS transits of TrES-3b occur later than the predictions of linear ephemeris of Mannaday et al. (2020). Similarly, the midtransit times of Qatar-1b derived from TESS light curves also appear to occur ~ 113.65 s later than predicted by the linear ephemeris of Su et al. (2021). Because of these timing differences, and the poor model fittings to timing data with $\chi_{\text{red}}^2 > 1$ above, we suspect the possibility of TTVs in both hot Jupiters. To explore this further, we obtained the timing residuals, $O - C$, by subtracting the midtransit times calculated using the derived ephemeris, T_m^c , from the observed midtransit times, T_m , for all the considered epochs, E . The estimated timing residuals are given in Table 6 (for TrES-3b) and Table 7 (for Qatar-1b), and are also depicted as a function of epoch E in Figure 4. The rms of the timing residuals of TrES-3b is ~ 65.56 s, while that of Qatar-1b is ~ 46.44 s.

4.2. A Periodicity Search for Additional Planets

To probe the periodicity in the timing residuals of both hot Jupiters that may be induced due to presence of an additional body, we computed generalized Lomb–Scargle periodograms (GLS; Zechmeister & Kürster 2009) for their timing residuals in the frequency domain. The resulting periodogram of TrES-3b is shown in the top panel of Figure 5. In this periodogram,

Table 4
The Best-fit Values of Parameters T_m , i , a/R_* , R_p/R_* , u_1 , and u_2 for 58 TESS Transit Light Curves of TrES-3b

Epoch (E)	T_m (BJD _{TDB})	i (deg)	a/R_*	R_p/R_*	u_1	u_2
3674	2458984.83927 ^{+0.00070} _{-0.00068}	81.84 ^{+0.14} _{-0.14}	5.921 ^{+0.052} _{-0.051}	0.1645 ^{+0.0072} _{-0.0063}	0.365 ^{+0.050} _{-0.050}	0.232 ^{+0.050} _{-0.050}
3675	2458986.14594 ^{+0.00080} _{-0.00077}	81.86 ^{+0.15} _{-0.14}	5.913 ^{+0.052} _{-0.052}	0.1598 ^{+0.0074} _{-0.0067}	0.363 ^{+0.050} _{-0.050}	0.229 ^{+0.050} _{-0.050}

(This table is available in its entirety in machine-readable form.)

Table 5
The Best-fit Values of Parameters T_m , i , a/R_* , R_p/R_* , u_1 , and u_2 for Our Two and 98 TESS Transit Light Curves of Qatar-1b

Epoch (E)	T_m (BJD _{TDB})	i (deg)	a/R_*	R_p/R_*	u_1	u_2
1388	2457618.62696 ^{+0.00024} _{-0.00023}	85.85 ^{+0.92} _{-0.71}	6.89 ^{+0.37} _{-0.30}	0.1464 ^{+0.0028} _{-0.0033}	0.565 ^{+0.046} _{-0.049}	0.165 ^{+0.049} _{-0.049}
1538	2457831.63075 ^{+0.00033} _{-0.00029}	83.04 ^{+0.46} _{-0.41}	6.01 ^{+0.20} _{-0.18}	0.1555 ^{+0.0024} _{-0.0024}	0.539 ^{+0.049} _{-0.049}	0.146 ^{+0.050} _{-0.049}

(This table is available in its entirety in machine-readable form.)

Table 6
Midtransit Times (T_m) and Timing Residuals ($O - C$) for 182 Transit Light Curves of TrES-3b

Epoch (E)	T_m (BJD _{TDB})	$O - C$ (days)	Transit Source	Timing Source	Dates Excluded from Timing Analysis
0	2454185.91110 ^{+0.00021} _{-0.00021}	-0.0000490	Sozzetti et al. (2009)	Mannaday et al. (2020)	
10	2454198.97359 ^{+0.00057} _{-0.00066}	0.0005782	Sozzetti et al. (2009)	Mannaday et al. (2020)	

References. Gibson et al. (2009), Sozzetti et al. (2009), Colón et al. (2010), Lee et al. (2011), Jiang et al. (2013), Kundurthy et al. (2013), Turner et al. (2013), Vaňko et al. (2013), Lee et al. (2011), Püsküllü et al. (2017), Ricci et al. (2017), Mannaday et al. (2020).

(This table is available in its entirety in machine-readable form.)

Table 7
Midtransit Times (T_m) and Timing Residuals ($O - C$) for 228 Transit Light Curves of Qatar-1b

Epoch (E)	T_m (BJD _{TDB})	$O - C$ (days)	Transit Source	Timing Source	Dates Excluded from Timing Analysis
0	2455647.63228 ^{+0.00031} _{-0.00033}	-0.0008948	von Essen et al. (2013)	Su et al. (2021)	
45	2455711.53484 ^{+0.00019} _{-0.00021}	0.0005704	Covino et al. (2013)	Su et al. (2021)	

References. von Essen et al. (2013), Maciejewski et al. (2015), Mislis et al. (2015), Collins et al. (2017), Su et al. (2021).

(This table is available in its entirety in machine-readable form.)

the highest peak of power, 0.1285, was found at the frequency of 0.01297 cycles epoch⁻¹, and the false-alarm probability (hereafter, FAP) corresponding to this highest power was 10%. This FAP was determined empirically, by randomly permuting the timing residuals to the observing epochs using a bootstrap resampling method with 10⁵ trials. The periodogram computed for the timing residuals of Qatar-1b is depicted in the bottom panel of Figure 5. Here, the highest peak power of 0.1640 was found at the frequency of 0.155942 cycles epoch⁻¹, and the corresponding FAP was 24%. In both periodograms, the estimated FAPs are found to be far below the threshold level of FAP = 5%, which means that short-term periodic TTVs in the timing residuals of both the hot Jupiters are not detected. Therefore, the possibility of an additional body in the orbits

close to both the hot Jupiters is ruled out. These findings are fully consistent with the previous results that are available in the literature (e.g., TrES-3: Kundurthy et al. 2013; Vaňko et al. 2013; Püsküllü et al. 2017; Mannaday et al. 2020, Qatar-1b: Maciejewski et al. 2015; Collins et al. 2017; Thakur et al. 2018; Su et al. 2021). The absence of short-term periodic TTVs in the timing residuals of both the hot Jupiters motivates us to explore the possibility of long-term TTVs, which may be induced due to either orbital decay or apsidal precession.

4.3. A Search for Orbital Decay

As mentioned above, the long-term TTVs in the hot-Jupiter systems may be produced by orbital decay (Levrard et al. 2009;

Table 8
The Uniform Priors and Best-fit Model Parameters for TrES-3b and Qatar-1b

Parameter	Uniform Prior		Best-fit Values with 1σ Uncertainties	
	TrES-3b	Qatar-1b	TrES-3b	Qatar-1b
<i>Linear Ephemeris</i>				
P (days)	(0, 2)	(0, 2)	$1.30618628^{+0.00000002}_{-0.00000002}$	$1.42002433^{+0.00000003}_{-0.00000003}$
T_0 [BJD _{TDB} - 2,450,000]	(4184, 4186)	(5646, 5649)	$4185.911149^{+0.000053}_{-0.000053}$	$5647.633175^{+0.000050}_{-0.000050}$
$a_f, \tau, N_{\text{eff}}$			$\sim 0.44, \sim 19, \sim 1052$	$\sim 0.44, \sim 18, \sim 1111$
$\chi^2, \chi^2_{\text{red}}(N_{\text{dof}})^a$			207.01, 1.63(127)	283.92, 1.56(182)
BIC			216.73	294.35
<i>Orbital Decay Ephemeris</i>				
P_q (days)	(0, 2)	(0, 2)	$1.30618610^{+0.00000012}_{-0.00000012}$	$1.42002386^{+0.00000014}_{-0.00000014}$
T_{q0} [BJD _{TDB} - 2,450,000]	(4184, 4186)	(5646, 5649)	$4185.911241^{+0.000079}_{-0.000079}$	$5647.633357^{+0.000073}_{-0.000073}$
$\frac{dP_q}{dE}$ (days) ^b	(-1, 1)	(-1, 1)	$0.87899^{+0.56241}_{-0.56517}$	$3.42245^{+1.01062}_{-1.01495}$
$a_f, \tau, N_{\text{eff}}$			$\sim 0.32, \sim 32, \sim 1000$	$\sim 0.32, \sim 35, \sim 914$
$\chi^2, \chi^2_{\text{red}}(N_{\text{dof}})$			204.12, 1.62(126)	271.50, 1.50(181)
BIC			218.70	287.14
<i>Apsidal Precession Ephemeris</i>				
P_s (days)	(0, 2)	(0, 2)	$1.30618619^{+0.00000008}_{-0.00000014}$	$1.42002379^{+0.00000020}_{-0.00000020}$
T_{ap0} [BJD _{TDB} - 2,450,000]	(4184, 4186)	(5646, 5649)	$4185.911740^{+0.000404}_{-0.000394}$	$5647.635063^{+0.00039}_{-0.000543}$
e	(0, 0.003)	(0, 0.005)	$0.00160^{+0.00096}_{-0.00105}$	$0.00410^{+0.00062}_{-0.00110}$
ω_0 [rad]	(0, 1)	(0, 1)	$0.41^{+0.37}_{-0.29}$	$0.23^{+0.25}_{-0.16}$
$\frac{d\omega}{dE}$ [rad/Epoch]	(0, 0.0005)	(0, 0.0005)	$0.000248^{+0.000144}_{-0.000155}$	$0.000439^{+0.000044}_{-0.000087}$
$a_f, \tau, N_{\text{eff}}$			$\sim 0.35, \sim 197, \sim 1015$	$\sim 0.41, \sim 166, \sim 1204$
$\chi^2, \chi^2_{\text{red}}(N_{\text{dof}})$			207.08, 1.67(124)	272.08, 1.52(179)
BIC			231.38	298.15

Notes.

^a N_{dof} is the number of degrees of freedom.

^b The uniform prior for δP is in days, while its best-fit value is in 10^{-10} days.

Matsumura et al. 2010; Penev et al. 2018). We thus explored this possibility for the TrES-3 and Qatar-1 systems. To do so, we followed Maciejewski et al. (2021) and fitted the following orbital decay model to the timing data of both the hot Jupiters:

$$T_q^c(E) = T_{q0} + P_q E + \frac{1}{2} \frac{dP_q}{dE} E^2, \quad (2)$$

where E is the epoch number, T_{q0} is the midtransit time at $E = 0$, P_q is the orbital period, $\frac{dP_q}{dE}$ is the change of orbital period in each orbit, and $T_q^c(E)$ is the calculated midtransit time. Here, we adopted the same procedure as employed in the case of the linear model fitting (see Section 3), except for running 32,000 steps per walker in the MCMC for deriving the best-fit ephemeris for the orbital decay model (i.e., $P_q, T_{q0}, \frac{dP_q}{dE}$). The best-fitting orbital decay ephemerides are given in Table 8. The timing residuals of the orbital decay ephemeris model were obtained by subtracting the midtransit times calculated using the linear ephemeris, $T_m^c(E)$, from those estimated using the orbital decay ephemeris, $T_q^c(E)$. The resulting timing residuals, $T_q^c(E) - T_m^c(E)$, are plotted as a function of epoch with the red dashed curves in the $O - C$ diagram of each hot Jupiter (see Figure 4). The brown solid lines depicted in the $O - C$ diagrams are 100 random draws from the posteriors of the orbital decay model, which are extrapolated for the next ~ 4.5 yr, to illustrate the future trend of the decay scenario. Using the

derived values of P_q and $\frac{dP_q}{dE}$ for TrES-3b and Qatar-1b, the period derivatives are calculated using $\dot{P}_q = \frac{1}{P_q} \frac{dP_q}{dE}$, and are found to be $\sim 2.12 \pm 1.92 \text{ ms yr}^{-1}$ and $\sim 7.60 \pm 3.19 \text{ ms yr}^{-1}$, respectively. Since these positive values of \dot{P}_q cannot be attributed to the orbital decay phenomenon, the observed change in the orbital period may be caused by another phenomenon, such as a third body in a wider orbit or apsidal precession (Patra et al. 2020).

4.4. A Search for Apsidal Precession

The previous theoretical work of Ragozzine & Wolf (2009) predicts that several hot Jupiters, such as WASP-4b, WASP-12b, CoRoT-1b, OGLE-TR-56b and TrES-3b, are good candidates for exploring the possibility of apsidal precession, if their orbits are at least slightly eccentric. Since the eccentricity of Qatar-1b is reported to be greater than the minimum threshold value of 0.003 ($e = 0.021^{+0.011}_{-0.010}$; Covino et al. 2013; $e \sim 0.012$; Bonomo et al. 2017), this hot Jupiter is a good candidate for an apsidal precession study. As the apsidal precession phenomenon can also produce long-term periodic TTVs in hot-Jupiter systems (see Ragozzine & Wolf 2009; Maciejewski et al. 2016; Patra et al. 2017; Bouma et al. 2019; Yee et al. 2020; A-thano et al. 2022), we probed the possibility of this phenomenon in the TrES-3 and Qatar-1 systems, by adopting the following apsidal precession model (Equation (3) of Mannaday et al. 2020, which was derived from Equations

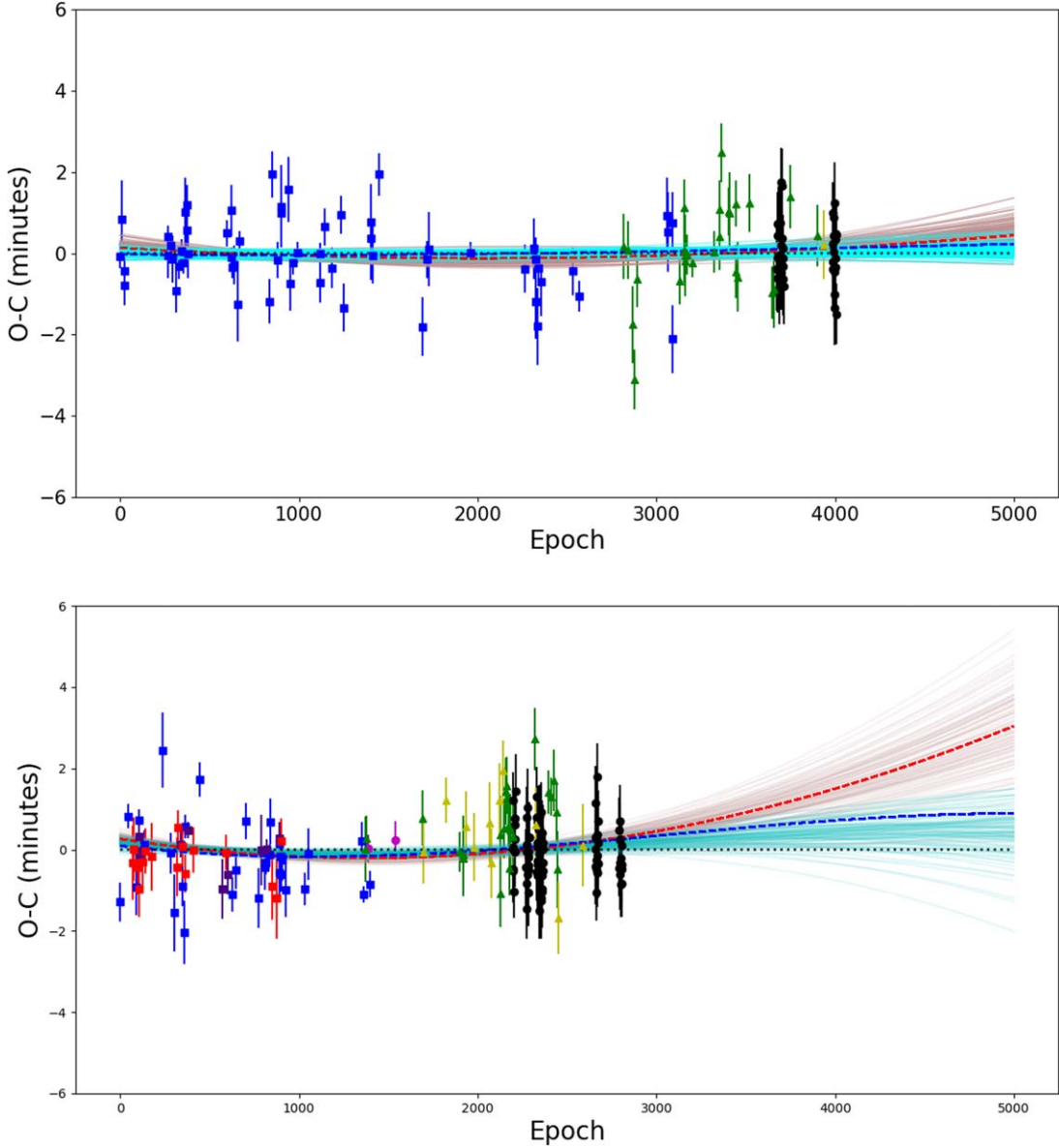


Figure 4. Top panel: $O - C$ diagram for the analysis of 129 midtransit times of TrES-3b. The black filled circles show the data from the TESS observations, the blue filled squares are from Mannaday et al. (2020), and the green and yellow filled triangles are from the quality 1 and quality 2 data of ETD. The dotted black line, dashed red curve, and dashed blue curve indicate the linear, orbital decay, and apsidal precession models, respectively. The lines show 100 random draws from the posteriors of the orbital decay (brown) and apsidal precession (cyan) models. The scenarios of both the models remain statistically indistinguishable in the time covered by current observations. The models are extrapolated for next ~ 4.5 yr, to illustrate the broad spectrum of possible solutions. Bottom panel: $O - C$ diagram for the analysis of 184 midtransit times of Qatar-1b. The magenta filled circles show the data from our observations, the black filled circles are for TESS observations, the blue filled squares are from Su et al. (2021), the indigo filled squares are from Mislis et al. (2015), and the red squares are from Collins et al. (2017). The other features of this panel are the same as described for the top panel.

(7), (9), and (10) of Patra et al. 2020):

$$T_{ap}(E) = T_{ap0} + P_s E - \frac{e P_s \cos(\omega_0 + E \frac{d\omega}{dE})}{\pi \left(1 - \frac{d\omega}{dE}\right)}, \quad (3)$$

where E is the epoch, $T_{ap}(E)$ is the calculated midtransit time, P_s is the sidereal period, e is the orbital eccentricity, ω is the argument of periastron, ω_0 is the argument of periastron at epoch zero ($E = 0$), and $\frac{d\omega}{dE}$ is the precession rate of periastron. We fitted the above model to the midtransit times of both the hot Jupiters as a function of epoch by following the procedure as described in Section 3, except for running 200,000 steps per walker in the

MCMC chains to determine the best-fit ephemeris of the apsidal precession model (i.e., $P_s, T_{a0}, e, \omega_0, \frac{d\omega}{dE}$). Initially, we tried to fit the model by considering wide ranges of uniform priors for the model parameters e, ω_0 , and $\frac{d\omega}{dE}$, but could not find reliable results, due to the nonconvergence of the MCMC chains. Therefore, we constrained the prior ranges to a shorter limit (as mentioned in Table 8) to obtain a reasonable fit. The results of the model fits obtained for both the hot Jupiters are listed in Table 8.

Similar to Mannaday et al. (2020), the derived values of the model parameters $e = 0.00160^{+0.00096}_{-0.00105}$, $\omega_0 = 0.41^{+0.37}_{-0.29}$ rad, and $\frac{d\omega}{dE} = 0.000248^{+0.000144}_{-0.000155}$ rad epoch $^{-1}$ are found to be statistically insignificant for TrES-3b. The reason for the statistically

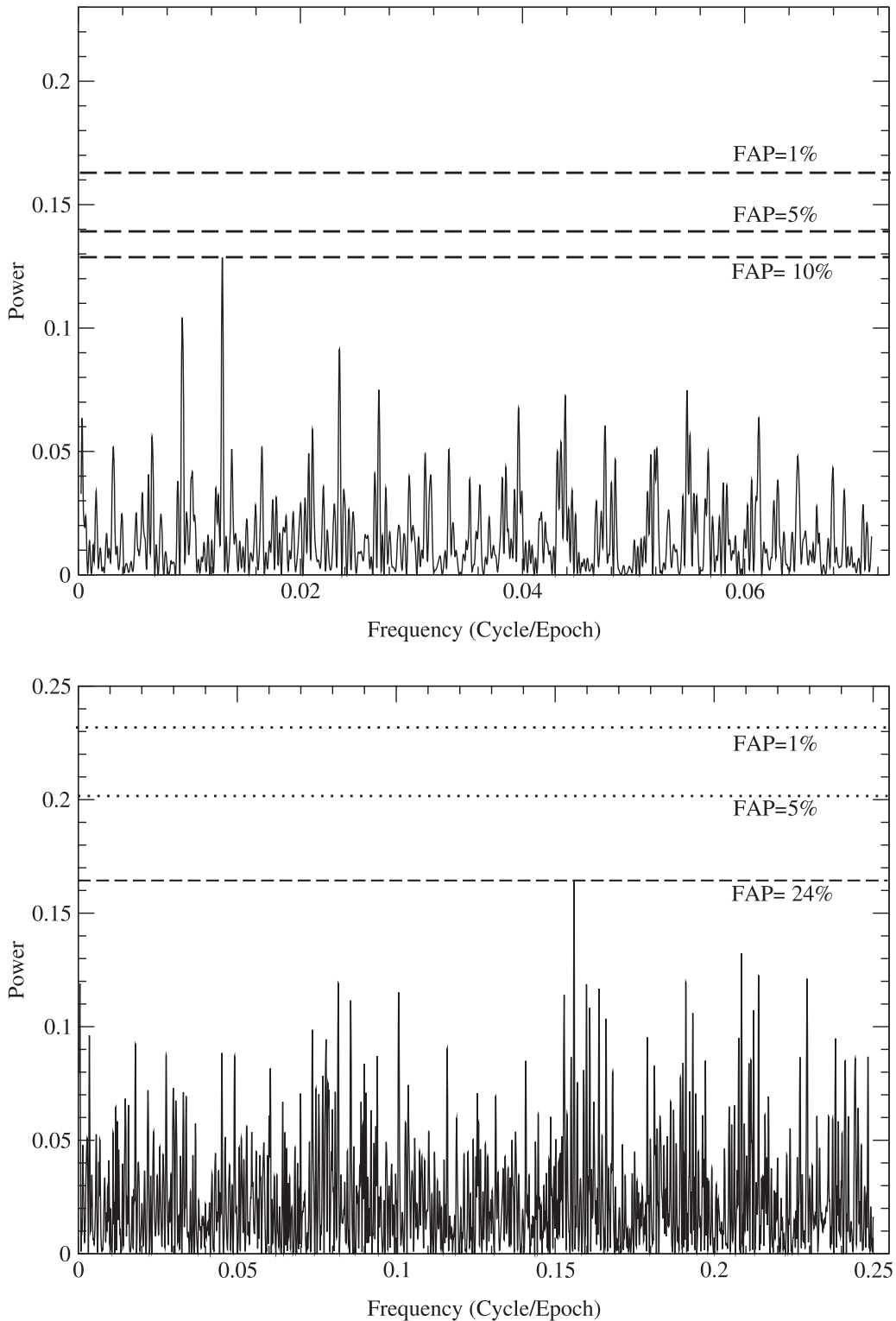


Figure 5. GLS periodograms computed for the timing residuals of TrES-3b (top panel) and Qatar-1b (bottom panel). The dashed line in each periodogram indicates the FAP level of the highest power peak. The dotted lines from top to bottom indicate the threshold levels of FAP = 1% and FAP = 5%, respectively.

insignificant results could either be due to a nearly circular orbit of TrES-3b, or a strong correlation between the model parameters, or by considering the wrong model for the timing data. Except for the less significant estimation of $\omega_0 = 0.23^{+0.25}_{-0.16}$ rad, the derived eccentricity of $e = 0.00410^{+0.00062}_{-0.00110}$ and the precession rate of $\frac{d\omega}{dE} = 0.000440^{+0.000044}_{-0.000087}$ rad epoch $^{-1}$ are found to be statistically

significant for Qatar-1b. The eccentricity of Qatar-1b derived here appears to be compatible with the 1σ upper limit ($e \sim 0.012$) reported in Bonomo et al. (2017).

Using the best-fit ephemeris derived for the apsidal precession and linear models, the timing residuals (i.e., $T_{ap}^c(E) - T_m^c(E)$) were calculated and are plotted as a function of epoch with the blue dashed curves in the $O - C$ diagrams of

TrES-3b and Qatar-1b (see Figure 4). In this figure, the solid cyan lines show 100 random draws from the posteriors of the apsidal precession model, which are extrapolated for the next ~ 4.5 yr, to show the future trend of the apsidal precession phenomenon. The random draws of TrES-3b suggest that the apsidal precession model is consistent with the linear model, whereas those of Qatar-1b appear to well represent the timing data considered. To confirm this, further high-precision photometric follow-up observations of the transits would be required.

5. Discussion

5.1. Constraints on the Stellar Tidal Quality Factor

Treating the observed $\frac{dP_q}{dE}$ of TrES-3b and Qatar-1b as a nondetection of orbital decay (see Section 4.3), one can place a constraint on the tidal quality factor Q'_* for the host stars of both hot Jupiters using the fifth percentile of the posterior probability distribution of $\frac{dP_q}{dE}$. To calculate Q'_* , we used the following equation, which is a modified form of the constant-phase lag model of Goldreich & Soter (1966):

$$Q'_* = -\frac{27}{2}\pi \left(\frac{M_p}{M_*}\right) \left(\frac{a}{R_*}\right)^{-5} \left(\frac{1}{\dot{P}_q}\right), \quad (4)$$

where P_q is the orbital period derived using the decay model, \dot{P}_q is the period derivative, $\frac{M_p}{M_*}$ is the mass ratio of the planet to the star, and $\frac{a}{R_*}$ is the ratio of the semimajor axis to the stellar radius. For the TrES-3 system, the values of the parameters $\frac{M_p}{M_*} = 0.001964$ and $\frac{a}{R_*} = 5.926$ are taken from Sozzetti et al. (2009). Corresponding to the fifth percentile of the posterior probability distribution of $\frac{dP_q}{dE}$, we derived $\dot{P}_q = -0.12 \text{ ms yr}^{-1}$ for TrES-3b. Substituting this \dot{P}_q and the values of the other parameters mentioned above, in Equation (4), we constrain the tidal quality factor of TrES-3 to be $Q'_* > 2.78 \times 10^6$, with 95% confidence (Maciejewski et al. 2018; Patra et al. 2020). As the fifth-percentile value of the posterior probability distribution of $\frac{dP_q}{dE}$ obtained for Qatar-1b is positive, we cannot place any constraint on Q'_* for Qatar-1.

5.2. Estimations of Planetary Love Numbers (k_p)

If we assume that the observed TTVs in both the hot-Jupiter systems are caused by apsidal precession, then the respective orbital eccentricities of TrES-3b and Qatar-1b would be $0.00160^{+0.00096}_{-0.00105}$ and $0.00410^{+0.00062}_{-0.00110}$, respectively (see Section 4.4). According to tidal evolution theory, the orbits of the hot Jupiters are expected to be circularized on a shorter timescale than the ages of their systems (Levrard et al. 2007; Dawson & Johnson 2018). Using Equation (17) of Patra et al. (2017) with an assumption of planetary tidal dissipation, $Q'_p = 10^6$, the estimated timescales for the tidal circularization of the orbits of TrES-3b and Qatar-1b are ~ 4 Myr and ~ 7 Myr, respectively. These timescales are several orders of magnitude smaller than the ages of their host stars (TrES-3: $0.6^{+2.0}_{-0.4}$ Gyr; Matsumura et al. 2010; Qatar-1: ~ 4 Gyr; Covino et al. 2013). As the timescales for tidal circularization are much smaller than the ages of the systems, the presence of an orbital eccentricity is inconsistent with tidal theory. If apsidal precession is taking

place in these systems, there must be some mechanism that can excite and maintain a nonzero eccentricity (see Bouma et al. 2019; Maciejewski et al. 2021). In this context, Ragozzine & Wolf (2009) showed that the interiors of very hot Jupiters could be a dominant source for apsidal precession. Since the apsidal precession rate is proportional to the planetary tidal Love number, k_p , a dimensionless parameter that depends on the interior density distribution of the planet, we adopted the following equation of Patra et al. (2017),

$$\frac{d\omega}{dE} = 15\pi k_p \left(\frac{M_*}{M_p}\right) \left(\frac{R_p}{a}\right)^5, \quad (5)$$

and estimated the value of k_p for both the hot Jupiters. By substituting the values of $\frac{d\omega}{dE}$ listed in Table 8, and other relevant parameters taken from Sozzetti et al. (2009) and Maciejewski et al. (2016), in Equation (5) above, we found $k_p = 0.61 \pm 0.12$ and $k_p = 1.95 \pm 0.26$ for TrES-3b and Qatar-1b, respectively. From the estimated $k_p = 0.61 \pm 0.12$, the interior density distribution of TrES-3b appears to be similar to that of Jupiter ($k_p = 0.59$: Wahl et al. 2016). As the obtained value of $k_p = 1.95 \pm 0.26$ for Qatar-1b is an unphysical value with a large uncertainty, it is difficult to infer the interior density profile of this hot Jupiter. This indicates a nondetection of apsidal precession using the available timing data of Qatar-1b (Maciejewski et al. 2021). To confirm this, future follow-up observations of transits and occultations will be needed.

5.3. Applegate Mechanism

It was proposed by Watson & Marsh (2010) that changes in the quadrupole moment of the host star (Applegate 1992) may also induce long-term TTVs in exoplanetary systems. Considering modulation periods of 11, 22, and 50 yr for magnetic activity cycles, they calculated the possible TTV amplitudes for many stars, including TrES-3. The largest TTV amplitude expected by them for TrES-3b due to an Applegate mechanism was $\delta t \sim 3.1$ s, which is an order of magnitude smaller than the TTV amplitude of ~ 32.26 s found by us (see Section 4.1). According to Equation (13) of Watson & Marsh (2010), the largest TTV amplitude that can be induced in the Qatar-1 system due to this mechanism over a modulation period of 50 yr would be $\delta t \leq 3$ s, which is much smaller than the TTV amplitude of ~ 113.65 s calculated by us (see Section 4.1). Therefore, an Applegate mechanism may not be a possible cause of TTVs in the TrES-3 and Qatar-1 systems.

5.4. Line-of-sight Acceleration

An accelerating motion of the center of mass of the star-planet system toward or away from the observer's line of sight can also change the observed orbital period of an extrasolar planet (see WASP-4b: Bouma et al. 2019; Southworth et al. 2019; Bouma et al. 2020; Turner et al. 2022; TrES-5b: Maciejewski et al. 2021). In contrast to orbital decay, the sign of the period change could either be positive or negative, depending on the direction of acceleration. Acceleration toward the observer causes a decreasing period, whereas an increasing period corresponds to acceleration away from the observer. If the centers of mass of the TrES-3 and Qatar-1 systems were really accelerating away from us with an amplitude \dot{v}_{RV} , then the observed \dot{P}_q of their hot Jupiters would be related to \dot{v}_{RV} by the

following equation of Maciejewski et al. (2021):

$$\dot{v}_{\text{RV}} = \frac{\dot{P}_q}{P_q} c, \quad (6)$$

where c is the speed of light and \dot{v}_{RV} is the linear trend in the RV of the host star. By substituting the derived values of P_q and \dot{P}_q (see Section 4.3) in Equation (6), the values of \dot{v}_{RV} are found to be $\sim 0.015 \pm 0.014 \text{ m s}^{-1} \text{ d}^{-1}$ and $\sim 0.051 \pm 0.021 \text{ m s}^{-1} \text{ d}^{-1}$ for TrES-3 and Qatar-1, respectively. In order to confirm this, the RV data for both the systems were collected from the literature (TrES-3: Sozzetti et al. 2009; Knutson et al. 2014; Qatar-1: Covino et al. 2013; Bonomo et al. 2017) and modeled using the *radvel* package (Fulton et al. 2018). The parameters of the RV semi-amplitude (K_b), the zeropoint velocity (γ), the linear trend in RV ($\dot{\gamma} = \dot{v}_{\text{RV}}$), and the jitter term (σ) were fitted freely. The orbital period and midtransit time were fitted under a Gaussian penalty, with their 1σ uncertainties from Mannaday et al. (2020) and Su et al. (2021). The remaining parameters, such as eccentricity (e), argument of periastron (ω), and quadratic trend in RV ($\ddot{\gamma}$), were fixed to zero. By analyzing the RV data of TrES-3, we find $\dot{\gamma} = 0.157 \pm 0.056 \text{ m s}^{-1} \text{ d}^{-1}$, which is 10 times larger than the abovementioned value of \dot{v}_{RV} . From this, it appears that the observed TTV in the TrES-3 system may not be due to line-of-sight acceleration. Since the value of $\dot{\gamma} = 0.046 \pm 0.008 \text{ m s}^{-1} \text{ d}^{-1}$ obtained from the RV data analysis of Qatar-1 is found to be consistent within a 1σ limit of the above estimated value of \dot{v}_{RV} , the acceleration of Qatar-1 away from our line of sight is a possible cause of the observed TTV. In order to confirm this, future high-precision RV observations of Qatar-1 will be required.

5.5. Possible Explanation for the Observed TTVs

For TrES-3b, the difference in the BIC between the apsidal precession and linear models is $\Delta\text{BIC} = \text{BIC}_{\text{precession}} - \text{BIC}_{\text{linear}} = 14.65$, with an approximate Bayes factor of $\exp(\Delta\text{BIC}/2) = 1517.77$. This ΔBIC provides strong evidence to rule out the possibility of apsidal precession in this planetary system (see Blečić et al. 2014; Maciejewski et al. 2016; Patra et al. 2017; Mannaday et al. 2020; Athano et al. 2022). This is also justified by the fact that the estimated value of the eccentricity, $e = 0.00160^{+0.00096}_{-0.00105}$, is very small, which would have a marginal effect on the midtransit times determined from the transit light curves (Maciejewski et al. 2016; Mannaday et al. 2020). As the $\Delta\text{BIC} = \text{BIC}_{\text{decay}} - \text{BIC}_{\text{linear}} = 1.97$ is found to be smaller than 2, it is difficult to clearly distinguish between the orbital decay and linear models (Collins et al. 2017). However, the positive and statistically less significant estimated value of \dot{P}_q (see Section 4.3), as well as the nondetections of an Applegate mechanism or line-of-sight acceleration in the TrES-3 system, enabled us to prefer the linear model to explain the transit time data of TrES-3b.

Based on the smaller values of χ_{red}^2 and BIC obtained from the orbital decay model fit, as compared to the other model fits (see Table 8), the orbital decay model appears to be the best model for the presently considered transit time data of Qatar-1b. However, we do not prefer this model, because the estimated positive value of \dot{P}_q indicates an increasing period. Due to having $\Delta\text{BIC} = \text{BIC}_{\text{precession}} - \text{BIC}_{\text{linear}} = 3.84$, with an

approximate Bayes factor of $\exp(\Delta\text{BIC}/2) = 6.82$, the linear model is somewhat preferable over the apsidal precession model for the considered transit time data of Qatar-1b. In addition to this, the unphysical value of k_p inferred from the observed precession rate (see Section 5.2) does not favor the presence of apsidal precession in the Qatar-1 system. From the RV data analysis of Qatar-1, it appears that the observed TTV of its hot Jupiter is caused by the line-of-sight acceleration of the system away from the Sun. However, future transit and RV observations of Qatar-1 would be valuable for clearly distinguishing between constant and increasing period phenomena.

6. Concluding Remarks

We present all the transit light curves of TrES-3b and Qatar-1b as observed by TESS in sectors 25, 26, and 40 and sectors 17, 21, 24, 25, 41, and 48, respectively. In addition to the TESS light curves, two more transits of Qatar-1b, observed by us, using a 1.23 m telescope, are presented. Since our aim was to refine the transit ephemeris and examine the possibility of TTVs in both systems, we have also collected the best-quality light curves from the ETD and the literature. In total, 182 transit light curves of TrES-3b and 228 transit light curves of Qatar-1b, spanning more than a decade, are employed in this work. Fitting a linear ephemeris model to the precisely estimated transit timing data, we have obtained refined orbital ephemerides for both systems. The derived ephemerides are fully consistent with previous results, but are estimated with improved precision (see Table 8). Our timing analysis indicates the possibility of TTVs in both hot Jupiters, which are unlikely to be short-term and periodic. This enables us to rule out the presence of additional planets in orbits close to TrES-3b and Qatar-1b.

Motivated by the above results, we have examined the possibilities of orbital decay and apsidal precession phenomena in both hot Jupiters. For TrES-3b and Qatar-1b, the respective positive period derivatives of $\dot{P}_q = 2.12 \pm 1.92 \text{ ms yr}^{-1}$ and $\dot{P}_q = 7.60 \pm 3.19 \text{ ms yr}^{-1}$ indicate nondetections of orbital decay in both the systems. However, we were able to constrain the lower limit of the tidal quality factor of TrES-3 to be $Q'_* > 2.78 \times 10^6$, with 95% confidence. We were not able to place a constraint on Q'_* for Qatar-1, because the 95% lower limit on \dot{P}_q is still positive. For TrES-3b, the value of k_p calculated with its observed precession rate of $\frac{d\omega}{dE} = 0.000248^{+0.000144}_{-0.000155} \text{ rad epoch}^{-1}$ is found to be 0.61 ± 0.12 . This value of k_p suggests that the interior density distribution of TrES-3b appears to be similar to that of Jupiter. Because of the statistically less significant estimated value of $\frac{d\omega}{dE}$, further high-precision transit observations are required to confirm the above inferred interior density profile of TrES-3b. Although the observed precession rate of Qatar-1b is statistically significant, the interior density profile of this hot Jupiter cannot be specified, because the inferred value of k_p is unphysical.

The Applegate mechanism is not a possible cause of the observed TTVs in both systems, since the largest TTV amplitudes expected from this mechanism are an order of magnitude smaller than the observed TTV amplitudes. Moreover, the observed TTV of TrES-3b does not appear to originate from line-of-sight acceleration, as the value of $\dot{\gamma}$ derived from the RV data is 10 times larger than \dot{v}_{RV} estimated using the observed \dot{P}_q . In contrast to TrES-3, the line-of-sight

acceleration of Qatar-1 is a possible explanation for the observed period change. In order to confirm our findings, we propose further photometric follow-up observations of the primary and secondary eclipse, as well as RV measurements of these hot-Jupiter systems. In this regard, it is worth mentioning that the ongoing TESS observations of the TrES-3 (sectors 52–53) and Qatar-1 (sector 51 and sectors 55–59) systems will be useful for shedding further light on the results obtained in this paper.

We thank the anonymous referee for useful comments that improved the quality of the paper. V.K.M. and P.T. thank the staff at IAO, Hanle, and CREST (IIA), Hosakote, for providing support during the previous observations of Qatar-1b and TrES-3b. P.T. expresses his sincere thanks to IUCAA, Pune, for providing support through the IUCAA Associateship Programme. P.T. and V.K.M. acknowledge the University Grants Commission (UGC), New Delhi, for providing financial support through Major Research Project No. UGC-MRP 43-521/2014(SR). J.S. and L.M. thank the staff at CAHA, Spain, for observational support. I.G.J. acknowledges funding from the Ministry of Science and Technology, Taiwan, through grant No. MOST 110-2112-M-007-035. This work was supported by the Slovak Research and Development Agency, under contract No. APVV-20-0148. This work was also supported by a VEGA grant of the Slovak Academy of Sciences, grant No. 2/0031/22. The research of P.G. was supported by an internal grant, VVGS-PF-2021-2087, of the Faculty of Science, P.J. Šafárik University, in Košice. L.M. acknowledges support from the “Fondi di Ricerca Scientificad’Ateneo 2021” of the University of Rome “Tor Vergata.” This paper includes data collected by the TESS mission, which are publicly available in the Mikulski Archive for Space Telescopes (MAST). The

contributors to the Exoplanet Transit Database (ETD) are gratefully acknowledged for making their transit light curves publicly available. While performing the timing analysis, the fruitful discussions and valuable suggestions that we received from D. Ragozzine and Kishore C. Patra are also acknowledged. We thank N. P. Gibson, J. W. Lee, D. Ricci, D. Mislis, and K. A. Collins for sharing their light curves with us. We also thank A. Sozzetti, K. D. Colón, P. Kundurthy, J. D. Turner, E. Covino, C. von Essen, and G. Maciejewski for making their transit light curves publicly available. This paper has made use of the VizieR catalog access tool, operated at CDS, Strasbourg, France, and NASA’s Astrophysics Data System Bibliographic Services.

Software: juliet (Espinoza et al. 2019), celerite (Foreman-Mackey et al. 2017), MultiNest (Feroz et al. 2009), PyMultinest (Buchner et al. 2014), TAP (Gazak et al. 2012), JKTLD (Southworth 2015), emcee (Foreman-Mackey et al. 2013), Radvel (Fulton et al. 2018), IPython (Pérez & Granger 2007), corner (Foreman-Mackey 2016), astroML (VanderPlas & Cannonly 2012), NumPy (Van Der Walt et al. 2011), and SciPy (Jones et al. 2001).

Appendix

TESS-observed Transit Light Curves of TrES-3b and Qatar-1b

The detrended TESS transit light curves of TrES-3b (black points) and the corresponding best fit TAP models (red curves) are shown in Figures A1–A2, while those of Qatar-1b are shown in Figures A3–A5. The epoch number (E) calculated corresponding to each transit event has been written at the bottom right of each panel of these figures.

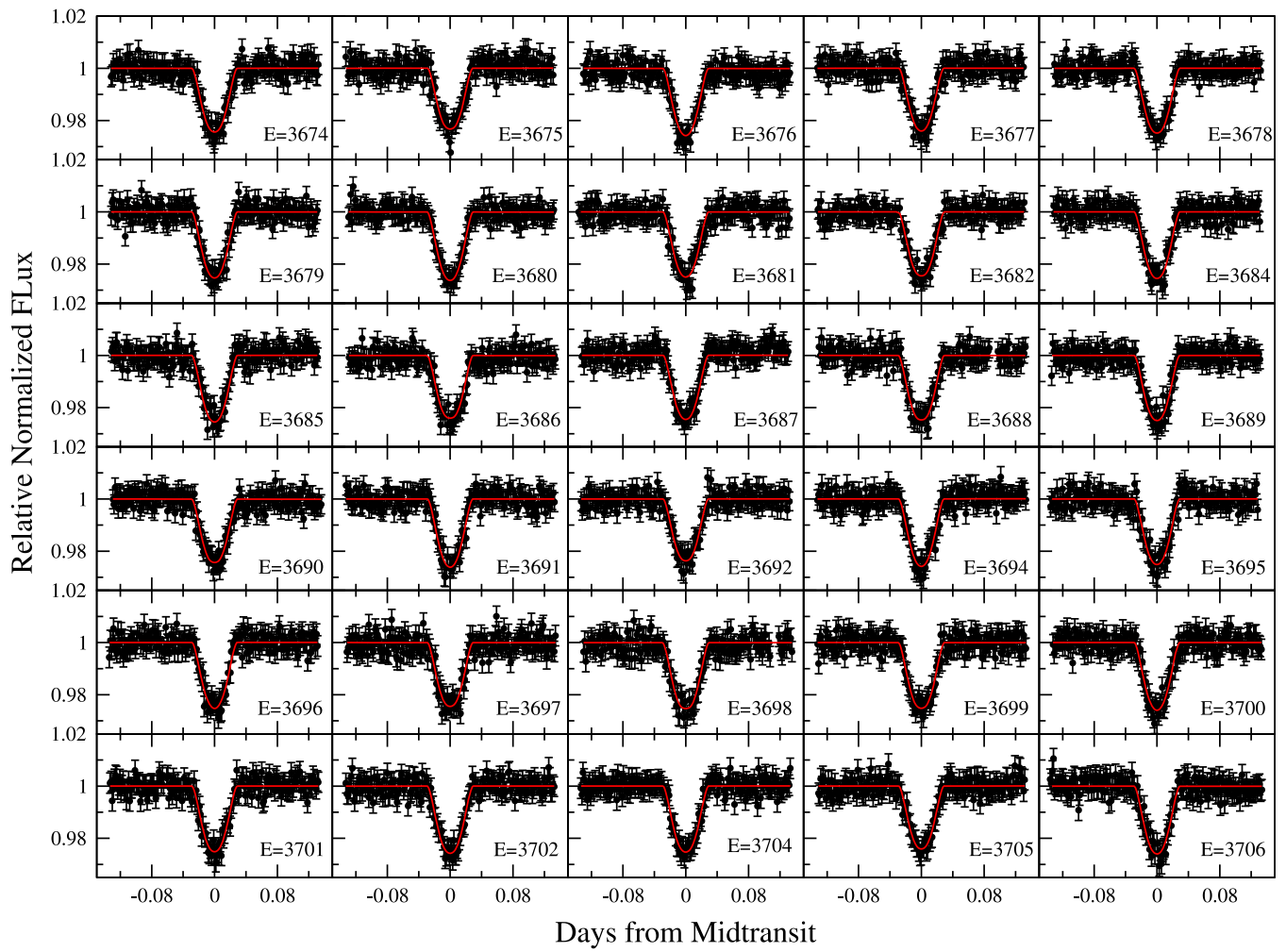


Figure A1. The normalized relative flux of TrES-3 as a function of the time (the offset from the midtransit time and in TDB-based BJD) of the individual transits observed by TESS: the points show the data, the solid lines show the best-fit models, and E is the calculated epoch number.

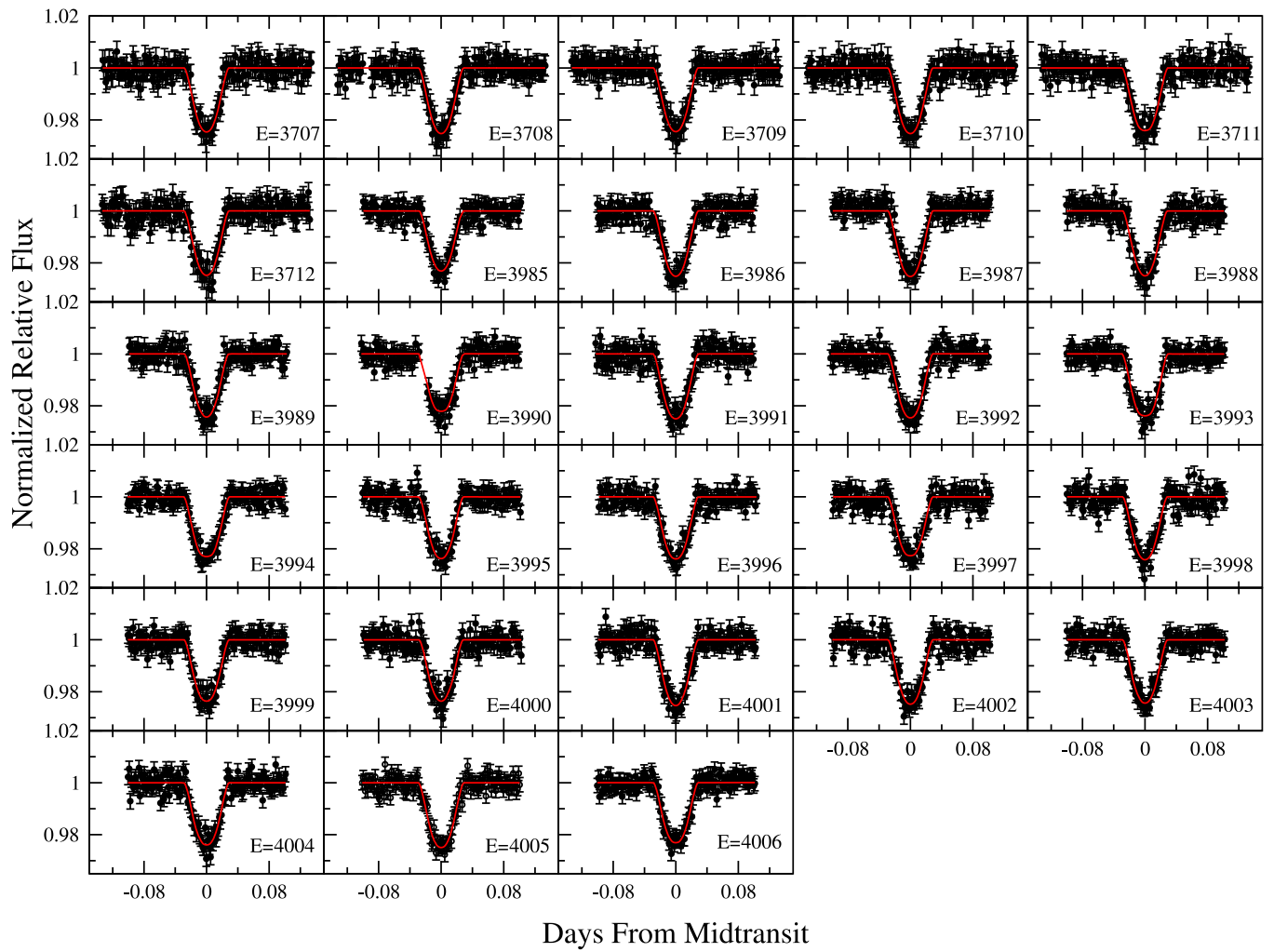


Figure A2. The same as Figure A1, but for the remaining epochs.

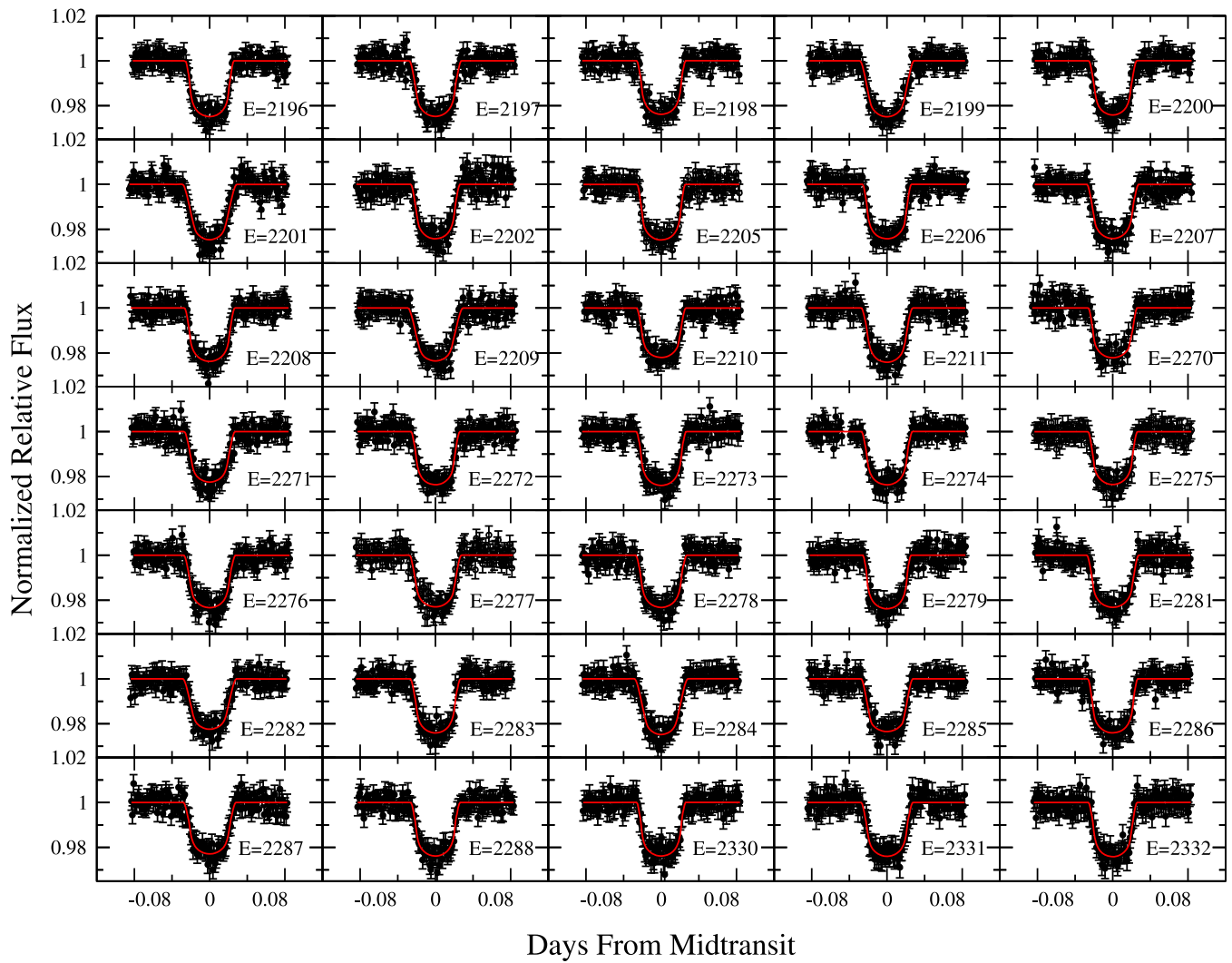


Figure A3. The normalized relative flux of Qatar-1 as a function of the time (the offset from the midtransit time and in TDB-based BJD) of the individual transits observed by TESS: the points show the data, the solid lines show the best-fit models, and E is the calculated epoch number.

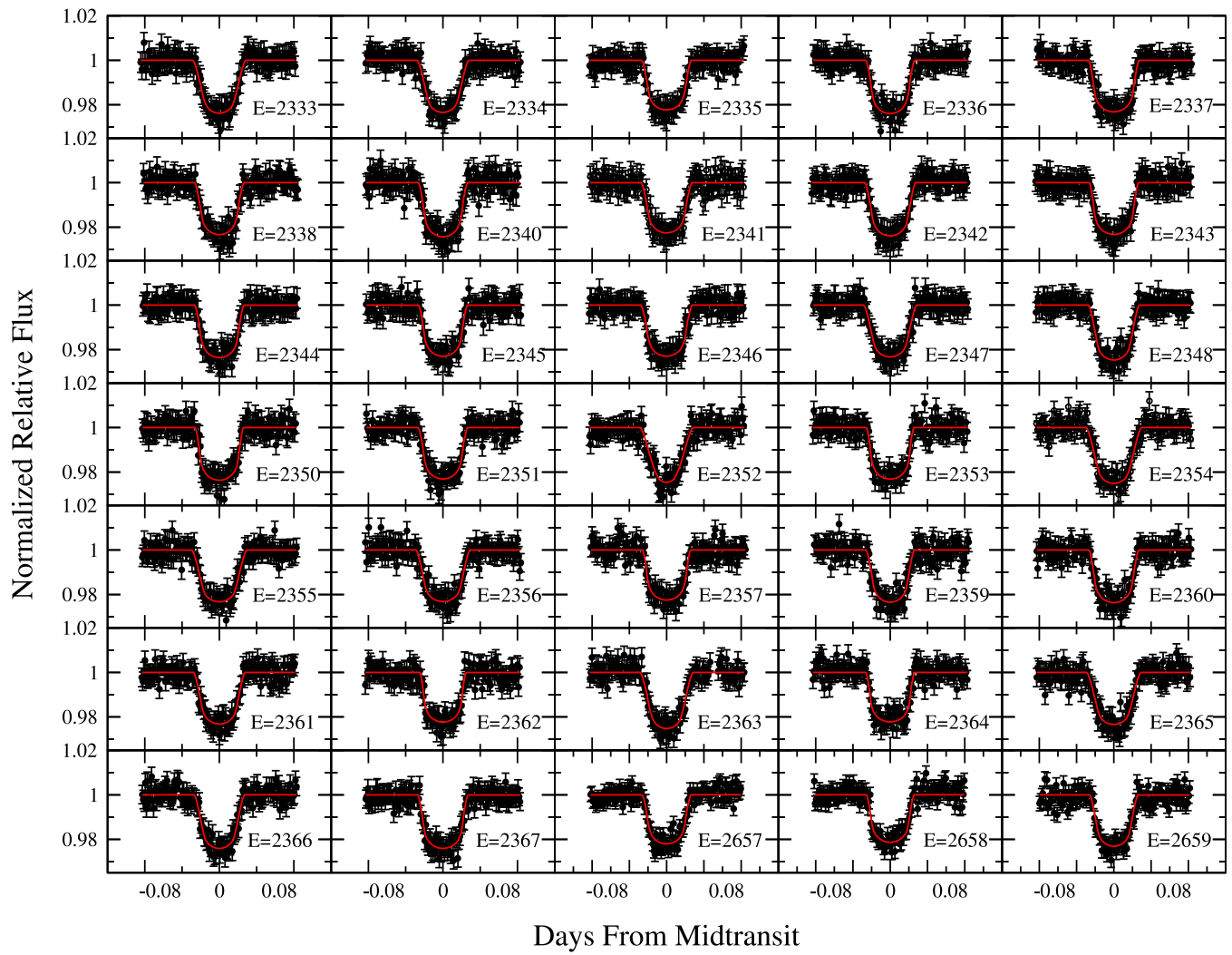


Figure A4. The same as the Figure A3, but for the remaining epochs.

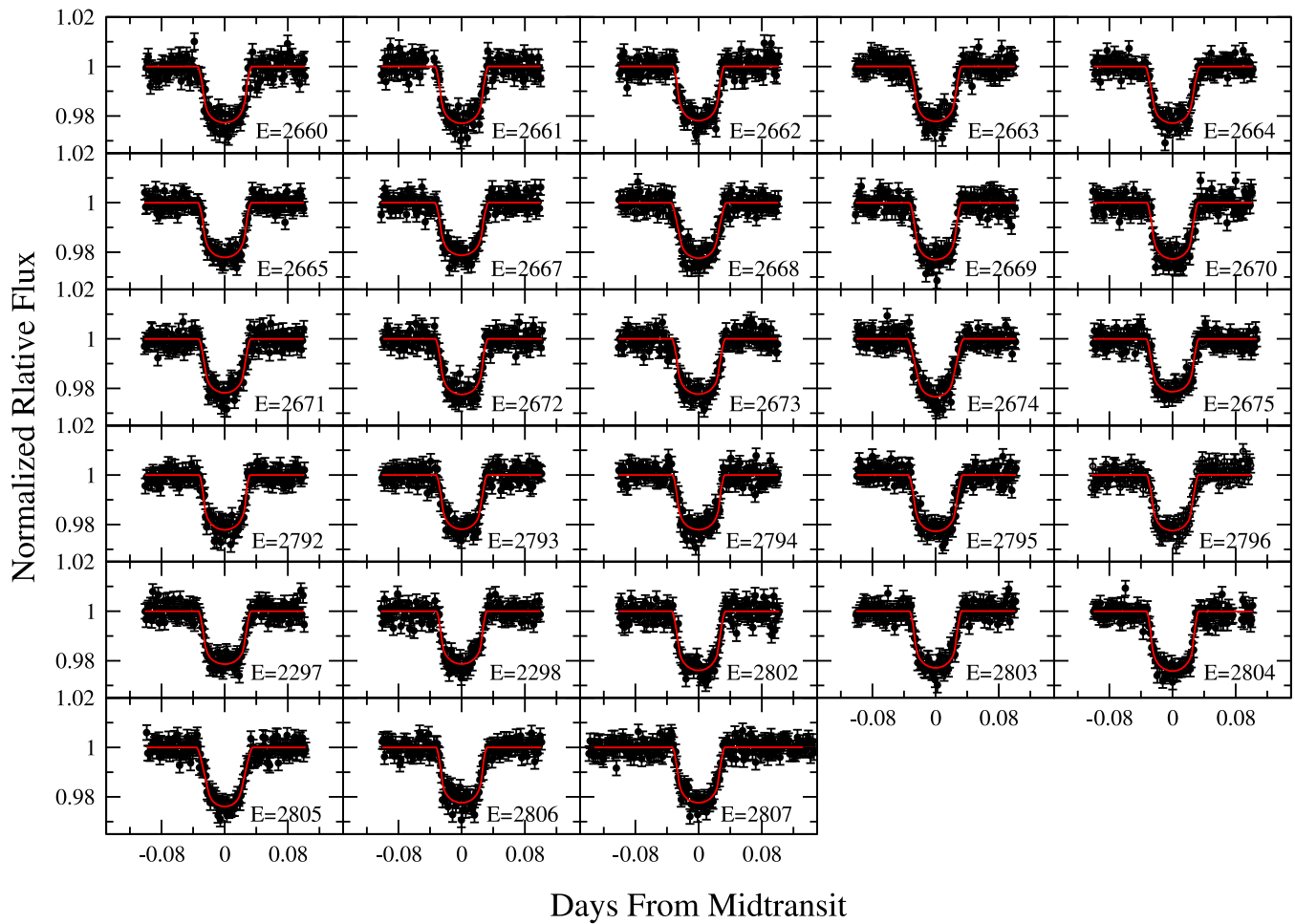


Figure A5. The same as the Figure A3, but for the remaining epochs.

ORCID iDs

Vineet Kumar Mannaday <https://orcid.org/0000-0002-0638-950X>
 Parijat Thakur <https://orcid.org/0000-0001-5958-0562>
 John Southworth <https://orcid.org/0000-0002-3807-3198>
 Ing-Guey Jiang <https://orcid.org/0000-0001-7359-3300>
 D. K. Sahu <https://orcid.org/0000-0002-6688-0800>
 L. Mancini <https://orcid.org/0000-0002-9428-8732>
 M. Vaňko <https://orcid.org/0000-0002-2798-6944>
 Emil Kundra <https://orcid.org/0000-0003-4005-9245>
 Pavol Gajdoš <https://orcid.org/0000-0003-1478-3256>
 Devesh P. Sariya <https://orcid.org/0000-0001-8452-7667>

References

Alsubai, K. A., Porely, N. R., Bramich, D. M., et al. 2011, *MNRAS*, **417**, 709
 Applegate, J. H. 1992, *ApJ*, **385**, 621
 Athano, N., Jiang, I.-G., Awiphan, S., et al. 2022, *AJ*, **163**, 77
 Battley, M. P., Kunimoto, M., Armstrong, D. J., et al. 2021, *MNRAS*, **503**, 4092
 Bleic, J., Harrington, J., Madhusudhan, N., et al. 2014, *ApJ*, **781**, 116
 Bonomo, A. S., Desidera, S., Benatti, S., et al. 2017, *A&A*, **602**, A107
 Bouma, L. G., Winn, J. N., Howard, A. W., et al. 2020, *ApJL*, **893**, L29
 Bouma, L. G., Winn, J. W., Baxter, C., et al. 2019, *AJ*, **157**, 217
 Buchner, J., Georgakakis, A., Nandra, K., et al. 2014, *A&A*, **564**, A125
 Claret, A. 2017, *A&A*, **600**, A30
 Claret, A., & Bloemen, S. 2011, *A&A*, **529**, A75
 Cloutier, R., & Triaud, A. H. M. J. 2016, *MNRAS*, **462**, 4018
 Collins, K. A., Kielkopf, J. F., & Stassun, K. G. 2017, *AJ*, **153**, 78

Colón, K. D., Ford, E. B., Lee, B., Mahadevan, S., & Blake, C. H. 2010, *MNRAS*, **408**, 1494
 Cortés-Zuleta, P., Rojo, P., Wang, S., et al. 2020, *A&A*, **636**, A98
 Covino, E., Esposito, M., Barbieri, M., et al. 2013, *A&A*, **554**, A28
 Davoudi, F., Bastürk, O., Yalçinkaya, S., et al. 2021, *AJ*, **162**, 210
 Dawson, R. I., & Johnson, J. A. 2018, *ARA&A*, **56**, 175
 Eastman, J., Gaudi, B. S., & Agol, E. 2013, *PASP*, **125**, 83
 Eastman, J., Siverd, R., & Gaudi, B. S. 2010, *PASP*, **122**, 935
 Espinoza, N., Kossakowski, D., & Brahm, R. 2019, *MNRAS*, **490**, 2262
 Feroz, F., Hobson, M. P., & Bridges, M. 2009, *MNRAS*, **398**, 1601
 Foreman-Mackey, D. 2016, *JOSS*, **1**, 24
 Foreman-Mackey, D., Agol, E., Angus, R., & Ambikasaran, S. 2017, *AJ*, **154**, 220
 Foreman-Mackey, D., Hogg, D. W., Lang, D., & Goodman, J. 2013, *PASP*, **125**, 306
 Fulton, B. J., Petigura, E. A., Blunt, S., & Sinukoff, E. 2018, *PASP*, **130**, 044504
 Garai, Z., Pribulla, T., Komžík, R., et al. 2020, *MNRAS*, **491**, 2760
 Gazak, J. Z., Johnson, J. A., Tonry, J., et al. 2012, *AdAst*, **2012**, 697967
 Gibson, N. P., Pollacco, D., Simpson, E. K., et al. 2009, *ApJ*, **700**, 1078
 Goldreich, P., & Soter, S. 1966, *Icar*, **5**, 375
 Goodman, J., & Weare, J. 2010, *CAMCoS*, **5**, 65
 Hoyer, S., Pallé, E., Dragomir, D., & Murgas, F. 2016b, *AJ*, **151**, 137
 Huang, C. X., Burt, J., Vanderburg, A., et al. 2018, *ApJL*, **868**, L39
 Huber, D., White, T. R., Metcalfe, T. S., et al. 2022, *AJ*, **163**, 79
 Ikwut-Ukwa, M., Rodriguez, J. E., Bieryla, A., et al. 2020, *AJ*, **160**, 209
 Jackson, B., Barnes, P., & Greenberg, R. 2009, *ApJ*, **698**, 1357
 Jenkins, J. M., Twicken, J. D., McCauliff, S., et al. 2016, *Proc. SPIE*, **9913**, 99133E
 Jiang, I.-G., Lai, C.-Y., Savushkin, A., et al. 2016, *AJ*, **151**, 17
 Jiang, I.-G., Yeh, L.-C., Thakur, P., et al. 2013, *AJ*, **145**, 68
 Jones, E., Oliphant, T., Peterson, P., et al. 2001, SciPy: Open Source Scientific Tools for Python, Available at: <http://www.scipy.org/>

- Knutson, H. A., Fulton, B. J., Montet, B. T., et al. 2014, *ApJ*, **785**, 126
- Kundurthy, P., Becker, A. C., Agol, E., Barnes, R., & Williams, B. 2013, *ApJ*, **764**, 8
- Lee, J.-W., Youn, J. H., Kim, S. L., Lee, C. U., & Koo, J. R. 2011, *PASJ*, **63**, 301
- Levrard, B., Correia, A. C. M., & Chabrier, G. 2007, *A&A*, **462**, L5
- Levrard, B., Winisdoerffer, C., & Chabrier, G. 2009, *ApJL*, **692**, L9
- Maciejewski, G., Dimitrov, D., Fernández, M., et al. 2016, *A&A*, **588**, L6
- Maciejewski, G., Dimitrov, D., Seeliger, M., et al. 2013, *A&A*, **551**, A108
- Maciejewski, G., Fernández, M., Aceituno, F., et al. 2018, *AcA*, **68**, 371
- Maciejewski, G., Fernández, M., Aceituno, F., et al. 2021, *A&A*, **656**, A88
- Maciejewski, G., Fernández, M., Aceituno, F. J., et al. 2015, *A&A*, **577**, A109
- Mancini, L., Southworth, J., Naponiello, L., et al. 2022, *MNRAS*, **509**, 1447
- Mannaday, V. K., Thakur, P., Jiang, I.-G., et al. 2020, *AJ*, **160**, 47
- Matsumura, S., Peale, S., & Rasio, F. A. 2010, *ApJ*, **725**, 1995
- Mislis, D., Mancini, L., Tregloan-Reed, J., et al. 2015, *MNRAS*, **448**, 2617
- O'Donovan, F. T., Charbonneau, D., Bakos, G. À., et al. 2007, *ApJL*, **663**, L37
- Paegert, M., Stassun, K. G., Collins, K. A., et al. 2021, arXiv:2108.04778
- Patra, K. C., Winn, J. N., Holman, M. J., et al. 2017, *AJ*, **154**, 4
- Patra, K. C., Winn, J. N., Holman, M. J., et al. 2020, *AJ*, **159**, 150
- Penev, K., Bouma, L. G., Winn, J. N., & Hartman, J. D. 2018, *AJ*, **155**, 165
- Pérez, F., & Granger, B. E. 2007, *CSE*, **9**, 21
- Petrucci, R., Jofré, F., Ferrero, L. V., et al. 2018, *MNRAS*, **473**, 5126
- Poddany, S., Brát, L., & Pejcha, O. 2010, *NewA*, **15**, 297
- Ragozzine, D., & Wolf, A. S. 2009, *ApJ*, **698**, 1778
- Rasio, F. A., Tout, C. A., Lubow, S. H., & Livio, M. 1996, *ApJ*, **470**, 1187
- Ricci, D., Sada, P. V., Navarro-Meza, S., et al. 2017, *PASP*, **129**, 064401
- Ricker, G. R., Winn, J. N., Vanderspek, R., et al. 2014, *Proc. SPIE*, **9143**, 914320
- Sariya, D. P., Jiang, I.-G., Su, L.-H., et al. 2021, *RAA*, **21**, 97
- Shan, S.-S., Yang, F., Lu, Y.-J., et al. 2021, arXiv:2111.06678
- Smith, J. C., Stumpe, M. C., Van Cleve, J. E., et al. 2012, *PASP*, **124**, 1000
- Southworth, J. 2015, JKTLD: Limb Darkening Coefficients, Astrophysics Source Code Library, ascl:1511.016
- Southworth, J., Barker, A. J., Hinse, T. C., et al. 2022, *MNRAS*, **515**, 3212
- Southworth, J., Dominik, M., Jørgensen, U. G., et al. 2019, *MNRAS*, **490**, 4230
- Southworth, J., Hinse, T. C., Burgdorf, M., et al. 2014, *MNRAS*, **444**, 776
- Southworth, J., Hinse, T. C., Jørgensen, et al. 2009a, *MNRAS*, **396**, 1023
- Püsküllü, Ç., Soyduğan, F., Erdem, A., & Budding, E. 2017, *NewA*, **55**, 39
- Sozzetti, A., Torres, G., Charbonneau, D., et al. 2009, *ApJ*, **691**, 1145
- Stassun, K. G., Oelkers, R. J., Paegert, M., et al. 2019, *AJ*, **158**, 138
- Stefansson, G., Mahadevan, S., Hebb, L., et al. 2017, *ApJ*, **848**, 9
- Stumpe, M. C., Smith, J. C., Catanzarite, J. H., et al. 2014, *PASP*, **126**, 100
- Stumpe, M. C., Smith, J. C., Van Cleve, J. E., et al. 2012, *PASP*, **124**, 985
- Su, L.-H., Jiang, I.-G., Sariya, D. P., et al. 2021, *AJ*, **161**, 108
- Szabó, G. M., Pribulla, T., Pál, A., et al. 2020, *MNRAS*, **492**, L17
- Tenenbaum, P., & Jenkins, J. 2018, TESS Science Data Products Description Document, EXP-TESS-ARC-ICD-0014 Rev D, <https://archive.stsci.edu/missions/tess/doc/EXP-TESS-ARC-ICD-TM-0014.pdf>
- Teske, J., Díaz, M. R., Luque, R., et al. 2020, *AJ*, **160**, 96
- Thakur, P., Mannaday, V. K., Jiang, I.-G., Sahu, D. K., & Chand, S. 2018, *BSRSL*, **87**, 132
- Turner, J. D., Flagg, L., Ridden-Harper, A., et al. 2022, *AJ*, **163**, 281
- Turner, J. D., Ridden-Harper, A., & Jayawardhana, R. 2021, *AJ*, **161**, 72
- Turner, J. D., Smart, B. M., Hardegree-Ullman, K. K., et al. 2013, *MNRAS*, **428**, 678
- Van Der Walt, S., Colbert, S. C., & Varoquaux, G. 2011, *CSE*, **13**, 22
- VanderPlas, J., Cannolly, A. J., Ivezić, Ž., & Gray, A. 2012, in Conf. Intelligent Data Understanding, ed. K. Das, N. V. Chawla, & A. N. Srivastava (Piscataway, NJ: IEEE), 47
- Vaňko, M., Maciejewski, G., Jakubík, M., et al. 2013, *MNRAS*, **432**, 944
- von Essen, C., Schröter, S., Agol, E., & Schmitt, J. H. M. M. 2013, *A&A*, **555**, A92
- Wahl, S. M., Hubbard, W. B., & Militzer, B. 2016, *ApJ*, **831**, 14
- Watson, C. A., & Marsh, T. R. 2010, *MNRAS*, **405**, 2037
- Wong, I., Shporer, A., Vissapragada, V., et al. 2022, *AJ*, **163**, 175
- Yee, S. W., Winn, J. N., Knutson, H. A., et al. 2020, *ApJL*, **888**, L5
- Zechmeister, M., & Kürster, M. 2009, *A&A*, **496**, 577